Antarctic Bottom Water from the Adélie and George V Land coast, East Antarctica (140-149°E)

Guy Darvall Williams, S. Aoki, S. S. Jacobs, S. R. Rintoul, T. Tamura, N. L. Bindoff

JOURNAL OF GEOPHYSICAL RESEARCH, VOL. 115, C04027, doi:10.1029/2009JC005812, 2010

Antarctic Bottom Water from the Adélie and George V Land coast, East Antarctica (140–149°E)

G. D. Williams,[1,2,3] S. Aoki,[1] S. S. Jacobs,[4] S. R. Rintoul,[2,5] T. Tamura,[1,2] and N. L. Bindoff[2]

Received 15 September 2009; revised 13 November 2009; accepted 20 November 2009; published 30 April 2010.

[1] We report on observations of dense shelf water overflows and Antarctic Bottom Water (AABW) formation along the continental margin of the Adélie and George V Land coast between 140°E and 149°E. Vertical sections and bottom layer water mass properties sampled during two RVIB *Nathaniel B Palmer* hydrographic surveys (NBP00–08, December 2000/January 2001 and NBP04–08, October 2004) describe the spreading of cold, dense shelf water on the continental slope and rise from two independent source regions. The primary source region is the Adélie Depression, exporting high-salinity dense shelf water through the Adélie Sill at 143°E. An additional eastern source region of lower-salinity dense shelf water from the Mertz Depression is identified for the first time from bottom layer properties northwest of the Mertz Sill and Mertz Bank (146°E–148°E) that extend as far as the Buffon Channel (144.75°E) in summer. Regional analysis of satellite-derived ice production estimates over the entire region from 1992 to 2005 suggests that up to 40% of the total ice production for the region occurs over the Mertz Depression and therefore this area is likely to make a significant contribution to the total dense shelf water export. Concurrent time series from bottom-mounted Microcats and ADCP instruments from the Mertz Polynya Experiment (April 1998 to May 1999) near the Adélie Sill and on the upper continental slope (1150 m) and lower continental rise (3250 m) to the north describe the seasonal variability in downslope events and their interaction with the ambient water masses. The critical density for shelf water to produce AABW is examined and found to be 27.85 kg m^{-3} from the Adélie Depression and as low as 27.80 kg m^{-3} from the Mertz Depression. This study suggests previous dense shelf water export estimates based on the flow through the Adélie Sill alone are conservative and that other regions around East Antarctica with similar ice production to the Mertz Depression could be contributing to the total AABW in the Australian-Antarctic Basin.

Citation: Williams, G. D., S. Aoki, S. S. Jacobs, S. R. Rintoul, T. Tamura, and N. L. Bindoff (2010), Antarctic Bottom Water from the Adélie and George V Land coast, East Antarctica (140–149°E), *J. Geophys. Res.*, *115*, C04027, doi:10.1029/2009JC005812.

1. Introduction

[2] Downslope overflows of dense shelf water off continental shelves are critical to the global ocean circulation and associated biogeochemical cycles [*Ivanov et al.*, 2004]. Around Antarctica, these occur when cold, dense shelf waters with sufficient negative buoyancy relative to the ambient water masses, spread down the continental slope to produce Antarctic Bottom Water (AABW) [*Price and Baringer*, 1994; *Baines and Condie*, 1998]. Around East Antarctica, the source of dense shelf water are discrete coastal polynya regions where there is intense atmospheric cooling and brine rejection from enhanced sea ice production.

[3] The abyssal layer circulation of the Australian-Antarctic Basin offshore of East Antarctica between 90°E and 150°E (Figure 1) is ventilated by two varieties of AABW [*Whitworth III*, 2002]. These are AABW from the Ross Sea that is advected westward from Cape Adare and locally formed AABW, most notably from the Adélie and George V Land (AGVL, 136°E–154°E) region, that is relatively colder, fresher and more oxygen rich [*Gordon and Tchernia*, 1972; *Rodman and Gordon*, 1982]. *Rintoul* [1998] showed the sudden shift in offshore bottom water properties west of 143°E and suggested the Adélie Depression and Mertz Glacier

[1]Institute for Low Temperature Science, Hokkaido University, Sapporo, Japan.
[2]Antarctic Climate and Ecosystem Cooperative Research Centre, Sandy Bay, Australia.
[3]Now at Laboratoire d'Ocanographie et du Climat: Exprimentations et approches numriques, UMR 7159, Universit Pierre et Marie Curie/MNHN, IRD, Institut Pierre Simon Laplace, CNRS, Paris, France.
[4]Lamont-Doherty Earth Observatory, Earth Institute at Columbia University, Palisades, New York, USA.
[5]Centre for Marine and Atmosphere Research, CSIRO, Hobart, Australia.

0148-0227/10/2009JC005812

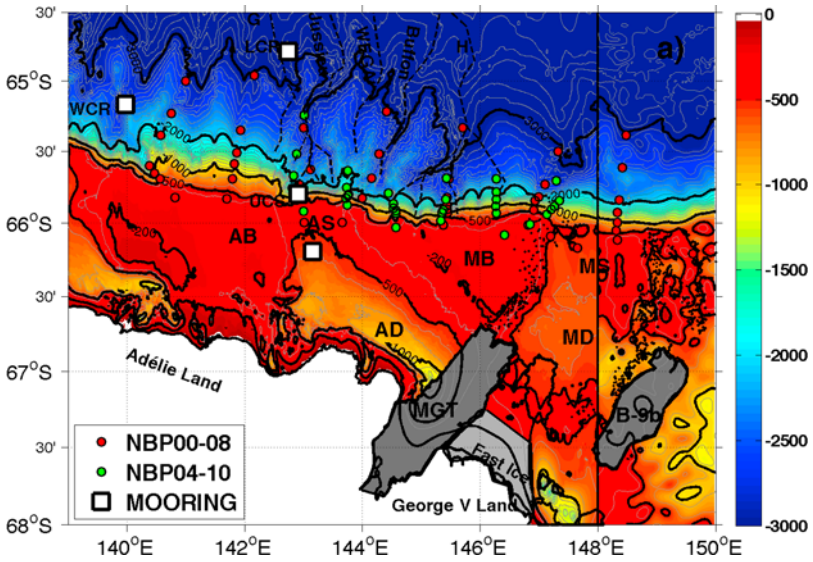

Figure 1a. The Adélie Depression and surrounding area with 500 m resolution (available at http://data.aad.gov.au/aadc/metadata/\metadata_redirect.cfm?md = AMD/AU/GVdem_2008). Bathymetry data east of 148°E from ETOPO1 (available at http://topex.ucsd.edu/marine_topo/). Major contour intervals shown for 4000, 3000, 2000, 1000, 500, and 200 m. The minor contour interval is 100 m and 200 m north and south of the 1000 m isobath, respectively. CTD stations from NBP00–08 (red) and NBP04–08 (green) as shown, with selected Mertz Polynya Experiment and JARE mooring locations (white squares). Channels from *Carbulotto et al.* [2006] as labeled. Features include the Adélie Bank (AB), Adélie Depression (AD), the Adélie Sill (AS), the Mertz Bank (MB), the Mertz Depression (MD), and Mertz Sill (MS). Glacial features include the Mertz Glacier (MGT), Iceberg B-9b, and a fast ice region east of the MGT. Grounded icebergs indicated by black dots.

polynya system (142°E–146°E, Figure 1b) as the major source of the locally formed AABW. In addition mooring observations on the continental rise near 140°E in 1995–1996 detected cold, bottom-intensified currents during winter and spring [*Fukamachi et al.*, 2000] and bottom CFC-11 values collected below 3400 m at this longitude during the "BROKE" survey in January–March 1996 found the highest circumpolar concentrations in the Australian-Antarctic Basin [*Orsi et al.*, 2002].

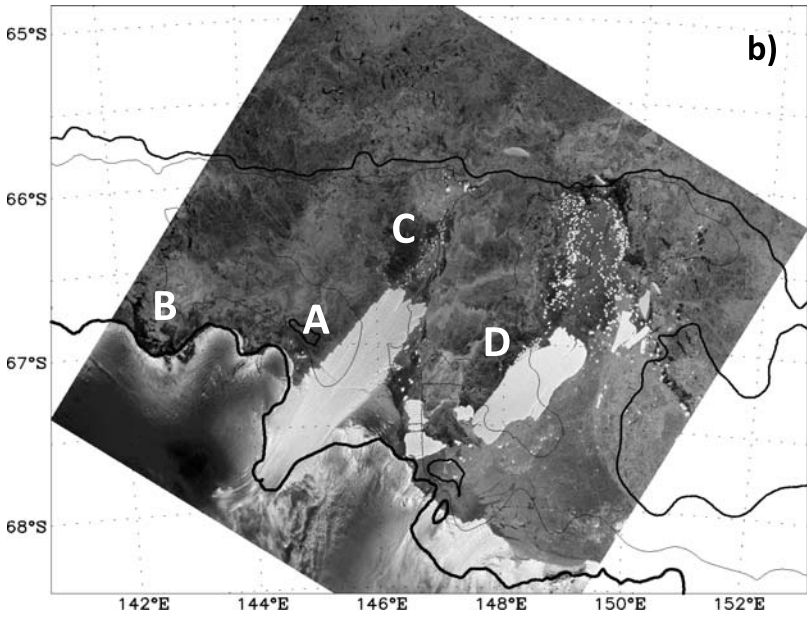

Figure 1b. ALOS PALSAR backscatter image of polynya regions east and west of the Mertz Glacier tongue on 5 September 2007. Polynya regions labeled A–D as described in the text.

[4] The Mertz Polynya Experiment (MPE, April 1998 to February 2000) described the first in situ observations of an Antarctic coastal polynya in winter [*Bindoff et al.*, 2001; *Williams and Bindoff*, 2003] and confirmed the Adélie Depression as a source of dense shelf water export. The MPE mooring deployments showed the seasonal cycle of water masses and formation of dense shelf water in the Adélie Depression available for export through the Adélie Sill [*Williams et al.*, 2008]. Modified Circumpolar Deep Water supplies the region over the shelf break and after a broad clockwise circulation and modification beneath polynyas along the western edge of the Mertz Glacier and around the coastal bays, 0.1–0.5 Sv of dense shelf water ($\sigma_\theta > 27.88$ kg m^{-3}) was estimated to be exported NNW through the Adélie Sill in 1998.

[5] Dense shelf water export is only one step in the Antarctic Bottom Water production process, as the mixing of downslope flows on the continental slope modifies the properties and volume transport through the entrainment/detrainment of ambient water masses [*Baines*, 2008]. As dense shelf water leaves the continental shelf, a geostrophic adjustment gives rise to a boundary front, known as the Antarctic Slope Front (ASF) [*Jacobs*, 1991; *Whitworth III et al.*, 1998], across which strong mixing occurs [*Baines and Condie*, 1998]. Sufficiently dense shelf water can penetrate the deep ocean as cascading plumes or gravity currents. The flow can also be steered down the slope by topographic features until it reaches equilibrium with its surroundings [*Baines and Condie*, 1998]. This is particularly relevant for the George V Land continental slope where a complex system of topographic channels exists [*Carbulotto et al.*, 2006; *De Santis et al.*, 2007], as shown in Figure 1a.

[6] The abyssal layer in the Australian-Antarctic Basin is reportedly becoming significantly colder and fresher [*Whitworth III*, 2002; *Jacobs*, 2004; *Aoki et al.*, 2005; *Jacobs*, 2006; *Rintoul*, 2007] and there has also been a concurrent freshening reported in the source regions for the AABW formed in the Ross Sea [*Jacobs et al.*, 2002; *Jacobs and Giulivi*, 2010]. Interpreting these changes in the context of climate change requires improved understanding of the mechanisms of bottom water production processes in each region. The comprehensive "AnSlope" studies in the western Ross Sea from 2003 to 2005 have detailed the dense shelf water overflows and AABW formation in this region [*Gordon et al.*, 2004, 2009; *Whitworth III and Orsi*, 2006; *Muench et al.*, 2009; *Padman et al.*, 2009] and there have been renewed observational programs conducted during the International Polar Year and beyond along the Adélie and George V Land (AGVL) margin.

[7] This paper describes for the first time detailed observations of dense shelf water overflows and AABW formation from two source regions on the AGVL margin using seasonal CTD surveys aboard the NB Palmer (January 2001 and October 2004, red and green circles in Figure 1a). A particular focus of this study is to follow up on the results from *Williams et al.* [2008] and investigate the fate of exported shelf water from additional MPE mooring deployments on the upper continental slope and lower continental rise north of the Adélie Sill in 1998–1999. Following the recent estimation of total ice production at all East Antarctic polynyas by *Tamura et al.* [2008] and the related dense shelf water export from modeling studies by *Marsland et al.* [2004, 2007], we seek generalizations from the mechanisms of dense shelf water overflows and AABW formation in this paper to better understand the potential for additional AABW input to the Australian-Antarctic Basin from these other regions.

[8] The background to the study region, data and methods utilized are detailed in section 2. In section 3 we describe the spreading of modified shelf water on the continental slope from the two ship-based surveys, revealing for the first time an additional source of dense shelf water from the Mertz Depression to the primary source region of the Adélie Depression. Section 4 presents the seasonal cycle of downslope flows and ambient water masses from the mooring observations on the upper slope and lower continental rise north of the Adélie Sill. In section 5 we compare the mechanisms for AABW production in this region with those detailed by the AnSlope study of the western Ross Sea. Regional ice production is examined from satellite analyses in discussion of the relative contribution to dense shelf water formation by the newly identified source region in the Mertz Depression. In particular we discuss the critical density of shelf water for AABW along the AGVL coast and the implications of these results for other East Antarctic polynya regions and their potential contribution to AABW in this sector.

2. Background

2.1. Adélie and George V Coasts (136°E–154°E)

[9] The Adélie Coast lies along East Antarctica between ~136 and 142°E, while the George V Coast extends eastward from there to ~154 E. The study area in this paper covers the region between 140°E and 149°E that is hereafter referred to as the Adélie and George V Land coast (AGVL). The adjacent continental shelf is dominated by a deep, glacially scoured trough formed by a larger predecessor to the Mertz Glacier, and has typically been called the Adélie Depression, bounded to the east by the Adélie Bank at 142°E. The floating extension of the present-day Mertz Glacier extends across the deepest part of that depression (>1300 m) and is currently grounded on the southern edge of the Mertz Bank [*Legrésy et al.*, 2004].

[10] A region of grounded icebergs north of the Mertz Glacier Tongue (MGT, Figure 1a) accumulates fast ice each winter. Together with the MGT, this feature forms the western boundary of a shallower deep to the east, sometimes referred to as the Mertz Trough or as in this paper, the Mertz Depression. The deeper of these two depressions leads to the relatively shallow (425 m) Adélie Sill, centered between 142.5°E and 143°E on the continental shelf break, while the shallower depression leads to a deeper (600 m) feature, centered between 147°E and 148°E, which we will call the Mertz Sill. The Mertz Sill is bounded to the east by the large grounded iceberg B-9b which calved from the Ross Ice Shelf in 1987 and settled in its current position in 1992 [*Massom*, 2003].

[11] Knowledge of the bathymetry of the AGVL continental margin has improved in recent years, in particular from high-resolution mapping with multibeam equipment aboard the NB Palmer [*Carbulotto et al.*, 2006; *De Santis et al.*, 2007]. These data have begun to detail the system of topographic channels bordered by steep ridges that are

50–200 m deep, up to 25 km wide and roughly extend down the upper continental rise from 2000 to 3000 m [*Carbulotto et al.*, 2006]. Only the southern extensions of the "Jussieu" and "H" channels cut the shelf break near the Adélie Sill 143°E and a minor depression less than 400 m deep within the Mertz Bank at 145°E [*Carbulotto et al.*, 2006].

2.2. Polynya Regions and Ice Production Estimates From Satellite

[12] There has been an ongoing regionalization of the polynya system along the AGVL coast as the resolution of available data and the focus of various studies has increased. Initially the entire Adélie Depression was treated as a single polynya, often referred to as the Mertz Glacier polynya [*Rintoul*, 1998; *Massom et al.*, 1998]. *Williams et al.* [2008] distinguish the Mertz Glacier "lee" polynya (denoted by locations "A" and "C" in Figure 1b) from the coastal "flaw" polynyas (location "B" in Figure 1b) of Watt and Commonwealth Bay. *Massom et al.* [2001] state that the two regions are forced by different wind regimes, the coastal polynyas primarily driven by a katabatic wind regime and the Mertz polynya more influenced by synoptic wind patterns. East of the Mertz Glacier Tongue, an additional "lee" polynya region is present over the Mertz Depression (location "D" in Figure 1b) as a result of the blocking effect of grounded iceberg B-9b and remnant icebergs from the latest breakup of the Ninnis Glacier Tongue.

[13] In this paper we examine the ice production over the different polynya regions west and east of the Mertz Glacier tongue, using estimates from a heat flux calculation using a thin ice algorithm for SSM/I Equal area Scalable Earth Grid (85 GHz and 37 GHz) data [*Tamura et al.*, 2007]. These data have been used to estimate ice production at all Antarctic polynya regions [*Tamura et al.*, 2008,] and in this paper we show results based on the NCEP-2 analysis as an upper bound and the ERA40 analysis as a lower bound. A simple linear relationship between the ERA40 and NCEP-2 annual totals over the ERA40 data period 1992–2001 is used to create the adjusted ERA40 totals over the NCEP-2 period from 1992 to 2005. This was done to provide comparison between the years where observations are available (1998, 2001, and 2004) and 2004 was outside the initial ERA40 data period.

2.3. Oceanographic Data and Methods

2.3.1. Summer (NBP00–08) and Spring (NBP04–08) CTD Surveys

[14] The shipboard CTD data in this paper comes from two U.S. surveys conducted in the AGVL region from the RVIB *Nathaniel B Palmer*. The first was an austral summer survey in December 2000 to January 2001, which we term NBP00–08. The second data set comes from the first part of the third US AnSlope cruise, conducted in the austral spring at the end of October 2004, which we term NBP04–08. Each survey conducted a series of cross-slope transects which we label from east to west J1–J7 for January (NBP00–08) and O1–O6 for October (NBP04–08). The summer survey covered a greater area than the spring survey, in particular extending west of the Adélie Sill and east of the Mertz Bank to the Mertz Sill, and so we present its description of the regional stratification and water masses first. The slope transects from the spring survey were inside the summer transects and did not extend as far down the continental rise.

[15] On both surveys a SeaBird 911plus system was used for the conductivity-temperature-depth (CTD) measurements. Dual temperature and conductivity sensors were sampled at a rate of 24Hz, with seawater pumped past the sensors. Dissolved oxygen was measured with a Clark-type Beckman oxygen electrode and on discrete water samples using Winkler titrations. CTD data were processed with Seasoft software, generally following standard procedures.

2.3.2. Water Masses of the AGVL Shelf and Continental Margin

[16] A schematic of the large-scale vertical distribution of water masses over the AGVL shelf and continental margin is shown in Figure 2, and includes a $\theta - S$ diagram of all NBP00-08 data with water mass boundaries as defined by originally by *Whitworth III et al.* [1998] and updated by *Orsi and Wierderwohl* [2009]. Offshore in the southern region of the Antarctic Circumpolar Current (ACC), the three main water masses from surface to bottom are cold Antarctic Surface Water (AASW), warm and saline Circumpolar Deep Water (CDW) and relatively cool and fresh Antarctic Bottom Water, with the commonly defined boundaries using the 28.00 and 28.27 kg m^{-3} neutral density (γ^n, *Jackett and McDougall* [1997]) surfaces, respectively.

[17] South of the Southern Boundary of the ACC, defined as the poleward extent of the subsurface 1.5°C isotherm, the CDW is termed "modified" Circumpolar Deep Water (mCDW). Moving poleward over the upper continental slope, the AASW layer thickens and the resulting subsurface horizontal density gradient across the permanent pycnocline between the AASW and the mCDW forms the Antarctic Slope Front (ASF) region. The ASF itself is commonly defined by the 0° isotherm, from its southernmost extent or position on the continental slope, to its northern extent where it becomes roughly parallel with the AASW/mCDW boundary.

[18] There is considerable variability in the structure of the ASF, in particular at the southern end. Classically, a "V-shaped" ASF indicates the production of AABW from a mixture of shelf water (SW), AASW, and mCDW [*Gill*, 1973]. SW is commonly defined as having the same neutral density as AABW ($\gamma_n > 28.27$ kg m^{-3}), but cooler than −1.85°C, following *Orsi and Wierderwohl* [2009]. Mixing across the shelf break ASF forms modified shelf water (MSW) that if sufficiently dense can be transported down the continental slope to form AABW. The MSW entrains warm, saline and less dense water from the ambient mCDW and therefore must be significantly denser than $\gamma_n > 28.27$ kg m^{-3} to form true AABW.

2.3.3. Mertz Polynya Experiment Moorings

[19] In addition to the ship-based CTD data, we present time series from moored instruments on the continental slope and rise from the Mertz Polynya Experiment (MPE). *Williams et al.* [2008] previously presented MPE mooring data from deployments in the Adélie Depression near the Mertz Glacier and in the AS, between April 1998 and February 2000. Figure 3 shows the linearly interpolated salinity and potential temperature for the Adélie Sill (AS) moorings at 454 m, chosen as the approximate minimum sill depth, from all available instruments previously presented by *Williams et al.* [2008] and includes potential density

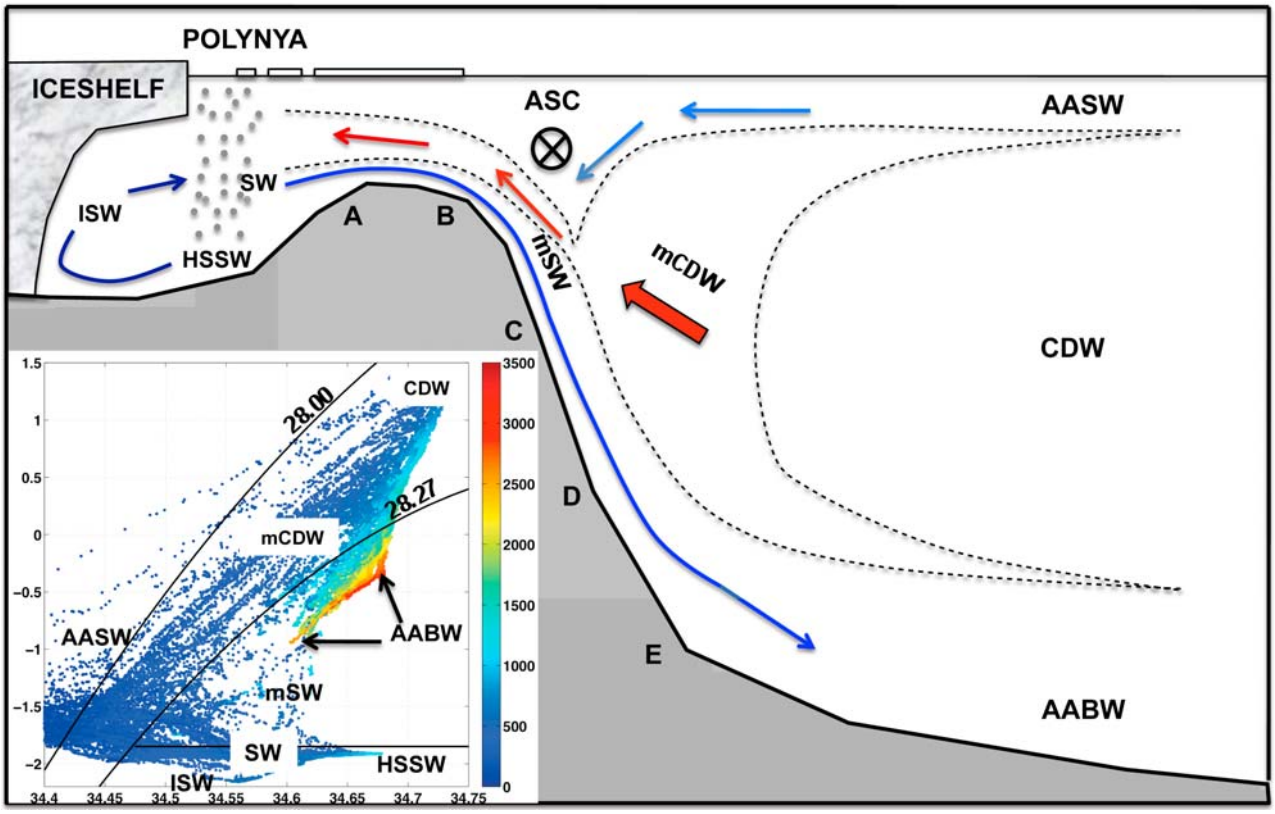

Figure 2. A 2-D schematic of the formation and export of dense shelf water and the downslope production of Antarctic Bottom Water (AABW) focusing on the Antarctic Slope Front. Labeled water masses and boundaries as described in the text. The Antarctic Slope Current is indicated by the circled "X." Inset: $\theta - S$ diagram of all CTD data from NBP00–08 shaded for depth and showing key water masses as defined by *Whitworth III et al.* [1998] and *Orsi and Wierderwohl* [2009]. Here, γ^n contours fitted to data labeled from NBP00–08 and NBP04–08 CTD stations and bounded by additional data from the Southern Ocean database.

(panel c). The time series of ADCP speed at 454 m in the same location is shown in Figure 3d.

[20] As reported by *Williams et al.* [2008], the water column is cooled to the near-surface freezing point in May–June. From June onward, the salinity and therefore density of the shelf water increases to a maximum in October greater than 34.7 and σ_0 = 27.95 kg m^{-3}, and then decreases to a minimum in April of less than 34.53 and σ_0 = 27.8 kg m^{-3}. The time series of current speed from the upward looking ADCP at 454 m in the AS location (Figure 3d) shows the 30 day running mean between 10 and 15 cm s^{-1} with episodic increases in the 2 day mean above 20 cm s^{-1} between June and February.

[21] Harmonic tidal analysis of the original 45 minute speed data using the *t_tide* package with nodal corrections [*Pawlowicz et al.*, 2002] found a combination of short-term (M2, O1, and K1) and long-term period (MF and MM) tidal constituents that each contributed between 1 and 2 cm s^{-1}. The same analysis was repeated for the Microcat data at this location but no short-term tidal constituents were found to be significant for salinity, θ or σ_0. This is substantially less tidal energy than found by modeling studies [*Erofeeva et al.*, 1997] and observations [*Whitworth III and Orsi*, 2006] near the shelf break of the western Ross Sea, where the O1 and K1 tides superimpose to form a 14 day spring-neap cycle with maximum tidal currents exceeding 1 ms^{-1} [*Padman et al.*, 2009].

[22] Importantly the AS mooring location was nearly 20 km south of the minimum sill depth and in their estimate of dense water export, *Williams et al.* [2008] presented upper and lower bounds based on a fixed export layer thickness between 100 and 200 m and the mean and maximum ADCP speed below the sill depth. The 2-D fluxgate compass proved useless in determining current direction due to the strong vertical component of magnetic field in the vicinity of the south magnetic pole, and *Williams et al.* [2008] assumed the ADCP speed measurements were directed out through the Adélie Sill based on the local bathymetry and the water mass properties recorded by the Microcats.

[23] In this paper we examine the fate of these exported dense shelf waters and present data from the remaining MPE mooring deployments on the Upper Continental Slope (UCS) and Lower Continental Rise (LCR) to determine the seasonal variability of the water masses and downslope mixing processes (see Table 1 for instrument details). Data from *Fukamachi et al.* [2000] at a Japanese mooring deployment (1995–1996) at the Western Continental Rise (WCR) location at 140°E will be discussed relative to the MPE data at the LCR location north of the Adélie Sill at

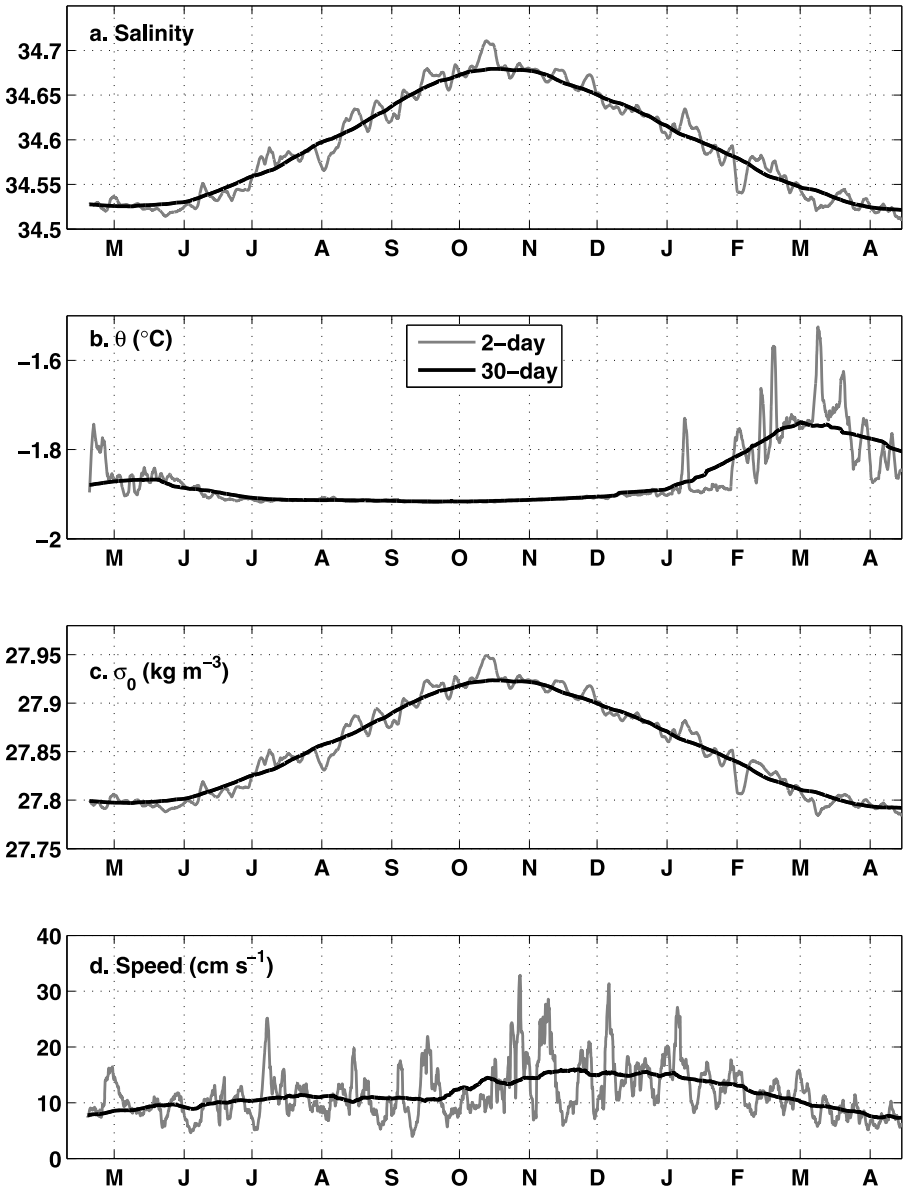

Figure 3. Seasonal variability of mean shelf water properties at the AS mooring site at 454 m. Time series of (a) salinity, (b) potential temperature (°C), (c) potential density (σ_0 kg m^{-3}), and (d) ADCP current speed (cm s^{-1}). Microcat data are interpolated from an array of moored instruments in this location during the Mertz Polynya Experiment from April 1998 to April 1999 (previously presented by *Williams et al.* [2008]) and shown as 2 day (gray line) and 30 day (black line) running means.

143°E. At the UCS mooring there was successful data retrieval from a bottom-mounted ADCP and two Microcats near the bottom. At the LCR mooring there was only valid data from a near-bottom Microcat M–380.

[24] The MPE mooring data presented in this paper underwent some post processing which is detailed in the work of *Rosenberg et al.* [2002] and *Williams et al.* [2008]. Due to the previously mentioned compass problems, the ADCP data at the UCS location is limited to current speed only. All Microcat data suffered from salinity spiking which was removed using a least squares inverse method that minimized the error associated with the temporal lag between the conductivity and temperature sensors. The impact of mooring "blow-down" was modeled and found to be negligible, in particular for instrument locations close to the bottom.

[25] There was a problem with salinity at the LCR mooring site, where Microcat 380 at 3196 m depth showed an initial offset (−0.0153) with respect to a CTD conducted after deployment and a freshening drift that exceeded the known seasonal variability of water masses in this region. This is attributed to contamination of the conductivity sensor by the turbidity currents in this region. We added the offset of 0.0153 to the entire record, and completed a linear detrending of the residual freshening signal which added a maximum 0.0227 to the end of the record. While this removed any interannual signal from the record, and decreased the accuracy of the absolute water mass property

Table 1. Mooring Locations and Instrument Details

Site	Location	Water Depth (m)	Instrument	Depth/Pressure (m)/(dbar)	Data Period
AS	66°12′S, 143°10′E	594	MPE Microcats *Williams et al.* [2008]	454	17/04/1998–11/04/1999
			ADCP−1143	589/596	17/04/1998–19/02/2000
UCS	65°48′S, 142°55′E	1180	Microcat−317	1139/1154	18/04/1998–14/05/1999
			Microcat−318	1157/1172	18/04/1998–14/05/1999
			ADCP−0135	1175/1190	17/04/1998–31/08/1999
LCR	64°47′S, 142°47′E	3213	Microcat−380	3196/3252	18/04/1998–14/05/1999
WCR	65°10′S, 139°59′E	2662	ACM−C	2632/2665	17th/01/1995–9/03/1996

values, we retain the time series as useful for detecting the extreme cold, fresh events that signal newly formed AABW at this location.

2.3.4. Assessing the Density of Overflows From the Continental Shelf to Rise

[26] Assessing the density of shelf water overflows is requisite in understanding the process of AABW formation. When examining water masses across a depth range from 500 m at the shelf break to 3000 m on the continental rise it becomes problematic using potential density at a fixed reference level due to the thermobaric effect that increases the influence of cold temperatures on density with increasing depth. When presenting the dense water outflow from the Ross Sea, *Muench et al.* [2009] used σ_{600} for selected AnSlope1 and AnSlope 2 data with a maximum depth of less than 2000 m, choosing 600 dbar as the reference pressure from the approximate sill depth. In this paper we have attempted to label the CTD and mooring data with neutral density values using the method of *Jackett and McDougall* [1997] with the CSIRO FORTRAN/Matlab routines (available at http://www.marine.csiro.au/jackett/NeutralDensity/).

[27] *Williams et al.* [2008] reported difficulties in accurately labeling neutral density surfaces south of the continental shelf break, and chose to present the export of dense shelf water in σ_θ classes. Indeed an examination of the error estimates from the CSIRO routines when applied to the data in this paper showed that for stations south of the 1000 m isobath on the continental slope there was an unacceptable level of uncertainty (>0.01 kg m^{-3}) across some middepth and bottom layer ranges. Therefore we will continue to use σ_0 for data locations in that range, which is convenient for comparison with the export estimates from *Williams et al.* [2008] and γ^n north of the 1000 m isobath, which is convenient for comparison between the CTD and mooring data on the slope and rise with respect to offshore estimates of AABW. To minimize the error in γ^n at the upper slope mooring we labeled the 2 day and 30 day running mean values of salinity and temperature only.

3. Overflows of Dense Shelf Water From the Adélie and Mertz Depressions

3.1. A General Description of the Bottom Layer

[28] Vertical profiles of water mass properties in the bottom layer at key locations (labeled A–E in Figure 2) that characterize the formation of AABW along the AGVL coast in summer are presented in Figure 4. These profiles summarize the variability of water mass properties for the modified shelf water and the ambient field at different depth regions on the continental shelf, slope and rise. At each location profiles are shown to highlight examples of bottom layers with strong, intermediate and weak/zero shelf water signatures (black, black dashed, and gray lines, respectively). Immediately south of the shelf break (location A) there is a homogenous bottom layer of cold, saline and oxygen-rich shelf water (black and black dashed lines), below varying strength incursions of warm, relatively fresh and oxygen-poor mCDW. In some locations however, the mCDW occupies the bottom layer and is more saline than the shelf water above (gray line).

[29] On the northern side of the shelf break (location B) there has already been a significant reduction in the thickness of the bottom layer (black and black dashed lines), with bottom values modified to warmer, more saline and oxygen-poor values. There is also a much warmer mCDW associated with the presence of the ASF as defined by the 0°C isotherm (gray line). On the upper continental slope near the 1000 m isobath (location C), the bottom layers with dense shelf water (black and black dashed lines) remain relatively thin and there is a strong gradient to the local mCDW above. There is also the first detection of intermediate density shelf water interleaving with the ambient mCDW (gray line) in an ~100 m thick cell 300 m above the bottom that is vertically unstable in neutral density.

[30] At the beginning of the continental rise near the 2000 m isobath (location D), the bottom layers have significantly changed, becoming thicker (100–200 m) and more homogenous with the stronger shelf water properties at locations B–C no longer present. There is some structure above the bottom layer at D (black and black dashed lines) that indicates the combination of two different bottom layers, with the less dense one having detached and appearing centered at 1800 m in both profiles. The warmer, more saline, oxygen deficient and vertically stable profile (gray line) is the ambient field. Finally on the lower rise (location E), we find bottom layers with the ambient AABW (gray line) and two "new" bottom water signals (black and black dashed lines). Detailed water mass properties at the bottom and averaged across the bottom layers at all stations on the continental slope presented hereafter are provided in Tables A1 and A2 in Appendix A.

3.2. Water Mass Properties Near the Shelf Break Between 142°E and 148°E

[31] The shelf water properties for summertime NBP00–08 CTD stations at, or near the deepest regions of the continental shelf break (i.e., sills) are shown in Figures 5a–5c. On the eastern flank of the Adélie Sill, stations 67 and 68 have a 50–100 m bottom layer of cold, oxygen-rich high-salinity (34.64–34.65) shelf water (σ_0 > 27.89 kg m^{-3}). There is a warming and decrease in oxygen concentration above 300 m marking the influence of a mCDW intrusion (also at station

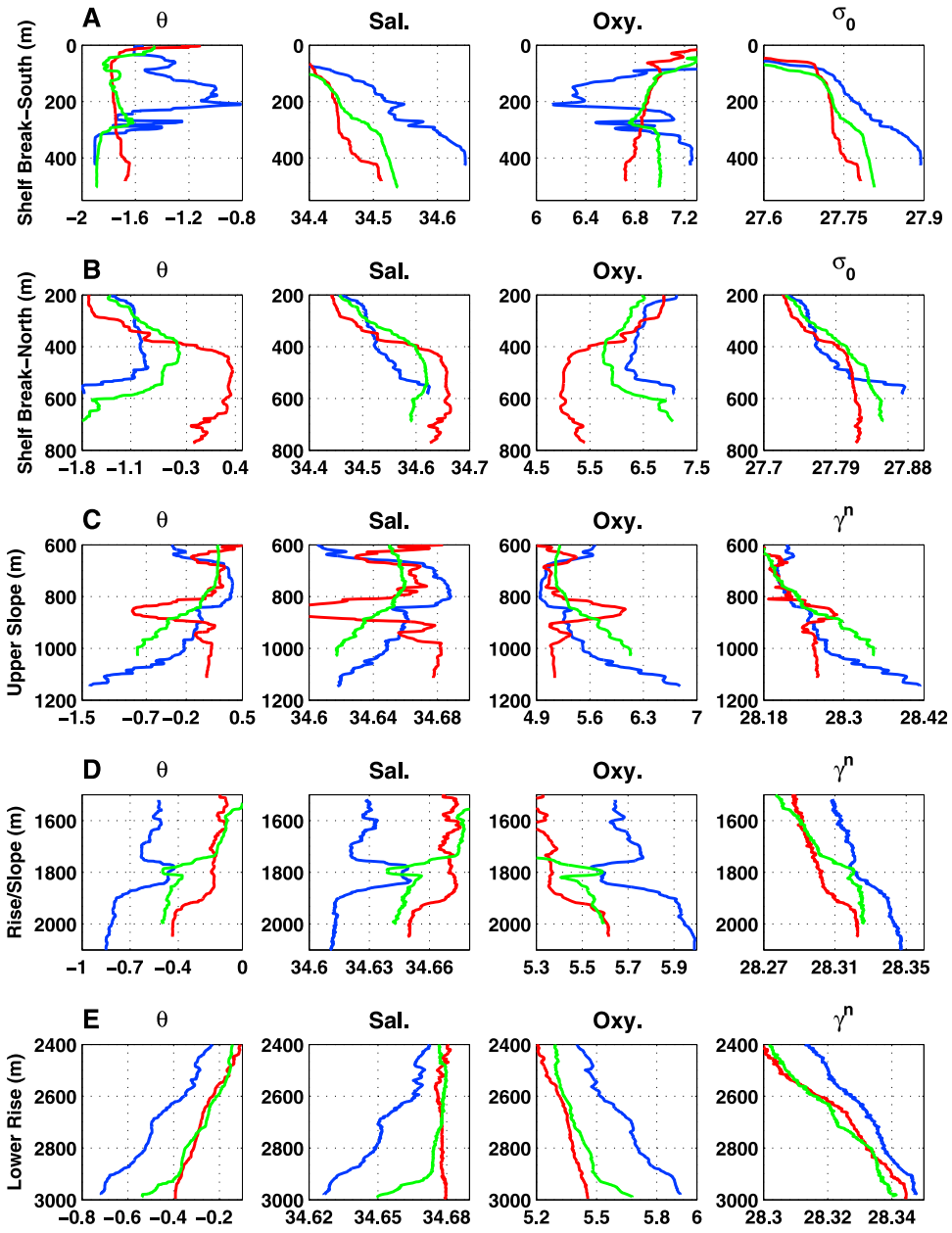

Figure 4. Examples of characteristic bottom layers at key locations in the export, modification, and downslope flow of dense shelf water. Data shown are vertical profiles of the bottom layer (left to right) at selected NBP00–08 CTD stations for potential temperature (θ °C), salinity, dissolved oxygen (ml l^{-1}) and density (kg m^{-3}). Profiles are grouped (top to bottom) at key locations (A–E) presented in Figure 2 in the downslope production of AABW from the southern shelf break (location A) to the continental rise (location E). Black and black dashed lines indicate stations with strong and weak modified shelf water properties, and gray stations indicate the ambient field, in particular the modified CDW and upstream AABW. Note the shift from potential density (σ_0) for locations A–B to neutral density (γ^n) for deeper locations C–E.

34 above 350 m). At station 69 and 20 on the western flank of the Adélie Sill there is little or no evidence of mCDW between 200 and 350 m. This is the same spatial distribution of mCDW across the Adélie Sill observed in July–August 1999 by *Williams and Bindoff* [2003], but is the reverse of the high-salinity shelf water signal below, which was strongest on the eastern side of the sill in summertime (bottom layer properties at stations 67 and 68 relative to stations 20 and 69) and stronger on the western side in winter.

[32] The large zonal coverage of the shelf break region by the NBP00–08 survey extended east of the Mertz Bank and grounded iceberg region at the northern end of the Mertz Glacier to the Mertz Depression and western flank of the

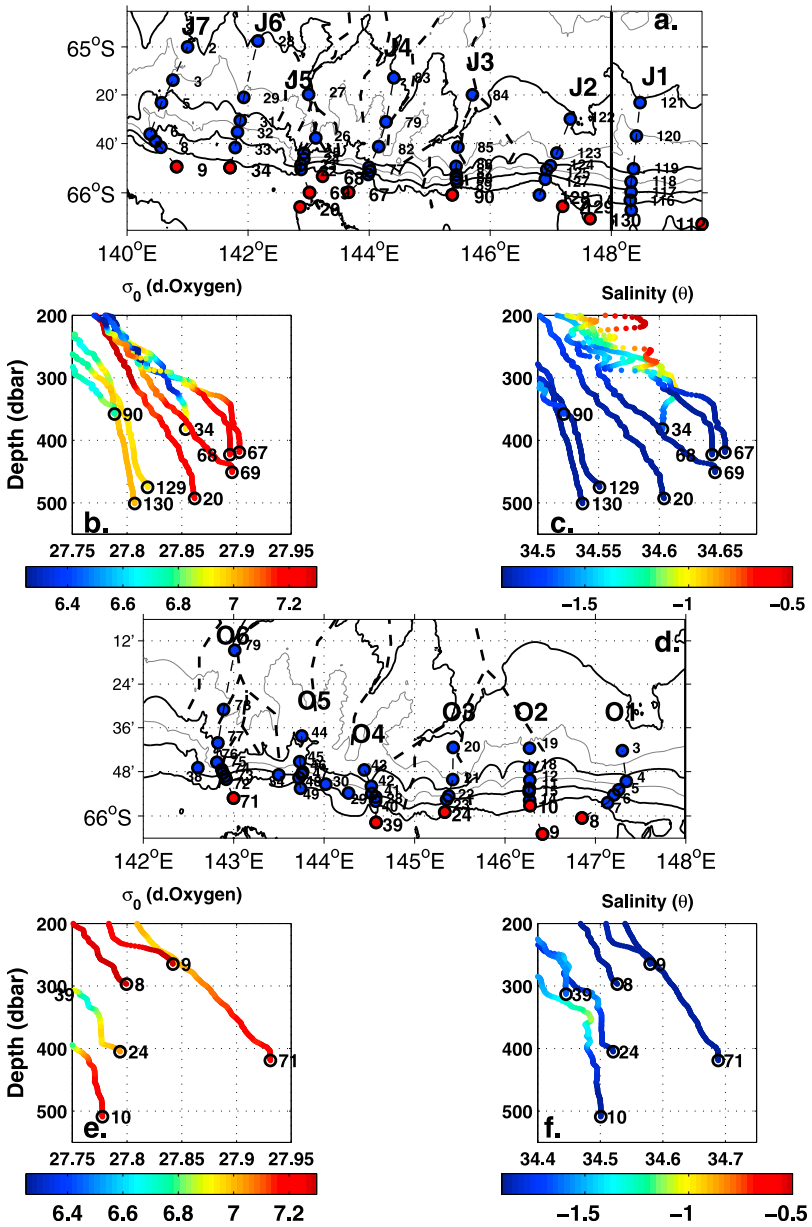

Figure 5. Zonal distribution of water mass properties along the shelf break. (a and d) The station layout for transects J1–J7 from NBP00–08 (Figure 5a) and O1–O6 from NBP04–08 (Figure 5d). Features labeled as in Figure 1a. Water mass properties for stations near the shelf break (larger circles, less than 550 m depth) are shown as vertical profiles of (b and e) potential density (σ_0 kg m^{-3}), and (c and f) salinity, shaded for dissolved oxygen (ml l^{-1}) and potential temperature (θ°C), respectively.

Ninnis Depression. On the western side of the Mertz Sill between 147°E and 148°E, stations 129–130 at the southern end of transect J2 showed a local shelf water maximum that was less dense (σ_0 > = 27.80 kg m^{-3}), fresher (34.53–34.55) and with lower oxygen concentration than observed near the Adélie Sill stations. There was only a weak mCDW signal in the upper layer above 300 m, with a decreased oxygen and freshening signal to the east at station 12 (not shown). Hereafter we refer to the higher-salinity shelf water in the Adélie Sill as the Adélie source and attribute the low-salinity dense shelf water on the eastern flank of the Mertz Sill to the Mertz Depression and call it the Mertz source. Following sections will examine the propagation of dense shelf water overflows from both these source regions.

[33] In the springtime survey of 2004 (NBP08–04) there was relatively less coverage of the shelf break region and no coverage of the Mertz source region. Nonetheless the high-salinity shelf water that was observed in the Adélie Sill (station 71) was more saline (34.69) and denser (σ_0 > = 27.93 kg m^{-3}) than observed in summer, with no mCDW signal above it. This is in agreement with the seasonal cycle reported by *Williams et al.* [2008], in particular the peak in

shelf water density in October and the increased influence of mCDW after December.

3.3. Large-Scale Distribution of Water Masses Over the Continental Slope and Rise

[34] Vertical sections of potential temperature from the across slope CTD transects in both summer and spring surveys (Figures 6 and 7) show the zonal variability in the meridional distribution of the water masses introduced in Figure 2. In summer the AASW layer, bounded by the 0°C isotherm in Figure 6 as a proxy for the ASF and offshore boundary between AASW and CDW, is coldest and largest on transect J1 and J7. The southward extension of the mCDW layer over the continental rise is strongest on transects J2–J3, but its influence onto the shelf break is strongest on transects J4–J6. The greatest variability is in the AABW layer, with its upper bound indicated by the γ^n = 28.27 kg m^{-3} density surface, and there is evidence of the downslope propagation of modified shelf water from both the Adélie and Mertz source regions.

[35] From transect J1 to J2/J3, and from J5 to J6 there is a distinct shoaling of the γ^n = 28.27 kg m^{-3} density surface on the upper slope. An ~200 m layer of cold modified shelf water (θ < −0.6 °C) is found below 2000 m on transect J6 northwest of the Adélie Sill, and to a lesser extent on transect J3 north of the Mertz Bank, with individual stations adjacent to these transects also showing a cold, dense modified shelf water signal (i.e., station 82 on transect J4 and station 27 on transect J5). The core bottom layer itself exceeds γ^n = 28.34 kg m^{-3} in both locations. Transect J4 at 144°E is unique with two interesting features: the interleaving of cool water (<−0.4°C) at intermediate depths (1000–1500 m at stations 77 and 79), and the bottom layer below which appears similar to the "double outflow" regime described by *Baines* [2008], whereby a secondary outflow region forms at an intermediate depth when less dense fluid rises out of the primary outflow region below.

[36] The vertical sections from cross-slope transects O1–O6 in spring 2004 (Figure 7) show some evidence of enhanced downslope transport of modified shelf water relative to summer 2001. Most noticeably the most extreme bottom layers of dense shelf water are now colder than −0.9° C, in particular at stations 44 and 77 on transects O5 and O6 northeast and north of the Adélie Sill region, respectively. Transect O6 also shows an ~40 km diameter eddy that appears to be exchanging warm mCDW with cool shelf water in the intermediate depth range between 500 and 1500 m and producing a doming in the γ^n = 28.27 kg m^{-3} density surface at station 77. Similar features appear to be present, though to a less extent, on transects O4 and O5. This eddy could be related to the cascade-induced upwelling proposed by *Kämpf* [2005], and its presence in October relative to January due to the increased dense shelf water overflow. Importantly this feature interrupts the structure of the Antarctic Slope Front in this location, but appears to still preserve the westward transport of the Antarctic Slope Current.

3.4. Propagation and Evolution of Modified Shelf Water From the Mertz and Adélie Sill Regions

[37] The propagation of dense shelf water properties on the continental slope from the Mertz and Adélie Sill source regions was examined using vertical profiles of neutral density and dissolved oxygen, together with $\theta - S$ diagrams for the 500 m bottom layer at offshore stations north of the 1000 m isobath (Figures 8 and 9). Once again we begin in summer 2001, in the east of the survey region, and follow the general direction of the Antarctic Slope Current westward across transects J1–J4 downstream of the Mertz Sill (Figure 8). As introduced earlier, the maximum shelf water densities in the eastern sector of the survey region were at stations 130 and 129 southeast of transect J2 on the western edge of the Mertz Sill. While there is no continuous downslope flow from this source and the temporal aliasing of the sampling is from west to east, there is a broad westward propagation and deepening of the oxygen-rich dense shelf signal from 1500–2000 m on transect J2 (stations 125, 124), to 2000–2500 m on transect J3 (stations 87, 86) to 2500 m and deeper on transect J4 (stations 82, 79 and 83). The strongest signal was at station 86 (160 m thick layer with θ = −0.8 °C and γ^n = 28.35 kg m^{-3}), and its influence on the offshore properties is found in the shift in $\theta - S$ properties to colder, fresher, oxygen-rich values at the station 83 on J4 (−0.54 °C, 34.65 and 5.68 ml l^{-1}), relative to stations 84, 122 and 121 to the east. The deep stations on transect J4 (82, 79 and 83) all follow the western flank of the "Buffon" channel which as mentioned earlier showed evidence of high-energy downslope activity in the sediment record.

[38] Continuing west into the vicinity of the Adélie source region there is a similar pattern of northwestward propagation of dense shelf water across transects J6 (stations 31, 29) and J7 (stations 5, 3 and 2) from the southern end of transect J5. There is also evidence of the northward transport of dense shelf water from the Adélie Sill to station 27 on transect J5 which is near the western flank of the Jussieu channel. The 80 m bottom layer at this station is the coldest (−0.7 °C), freshest (34.63) and most oxygen-rich (5.89 ml l^{-1}) of all stations near the 3000 m isobath. At the same depth but one transect to the west, station 28 has a weak local AABW signal (i.e., fresher, colder, more oxygen) over 100 m above the bottom layer of ambient AABW previously sampled on transects J1–J3. This demonstrates that in the upper layer of AABW between 2500 and 3000 m depth, the downslope events that are less dense than the ambient AABW (i.e., 28.34 kg m^{-3}) will detach from the continental rise. This is important because below 2500 m and the γ^n = 28.27 kg m^{-3} density surface, these events are technically still contributing to the AABW layer, but their influence is limited to the upper levels above the abyssal layer of the Australian-Antarctic Basin.

[39] The spring survey covered a smaller area over a shallower depth range with little repetition of the summer CTD stations. In considering the bottom layer properties from the spring survey (Figure 9), we anticipate that in following with the seasonal cycle of dense shelf water export from the Adélie Depression which peaks in October, and notwithstanding large interannual variability between 2000 and 2004, the downslope "events" on the continental slope during spring (NBP04–08) should be thicker, in greater number and colder, saltier, denser and more oxygen rich than in summer. However this is not clear from the data shown in Figure 9. As shown in Figure 7, there are colder bottom layers in October, but overall the layers appear to be less

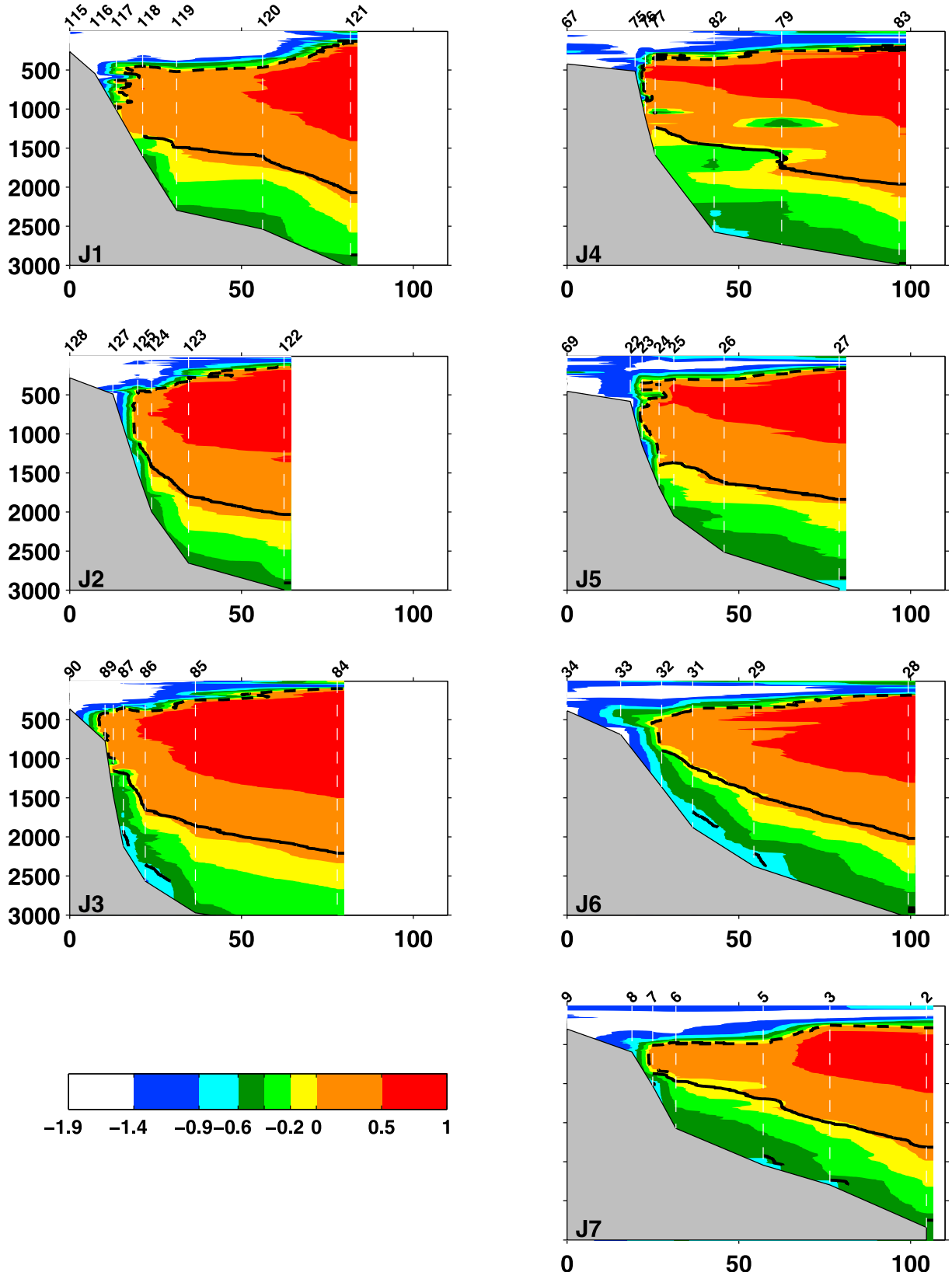

Figure 6. Vertical sections of potential temperature (°C) along meridional transects J1–J7 from summer 2001 (NBP00–08, Figure 5a). Abscissa is distance (km); ordinate is depth (dbar). Shaded contours as shown. Thick black lines are neutral density (γ^n) contours 28.27 and 28.34 kg m^{-3} for stations greater than 1000 m in depth. Dashed black lines are the 0°C isotherm indicating the Antarctic Slope Front. Station numbers as shown.

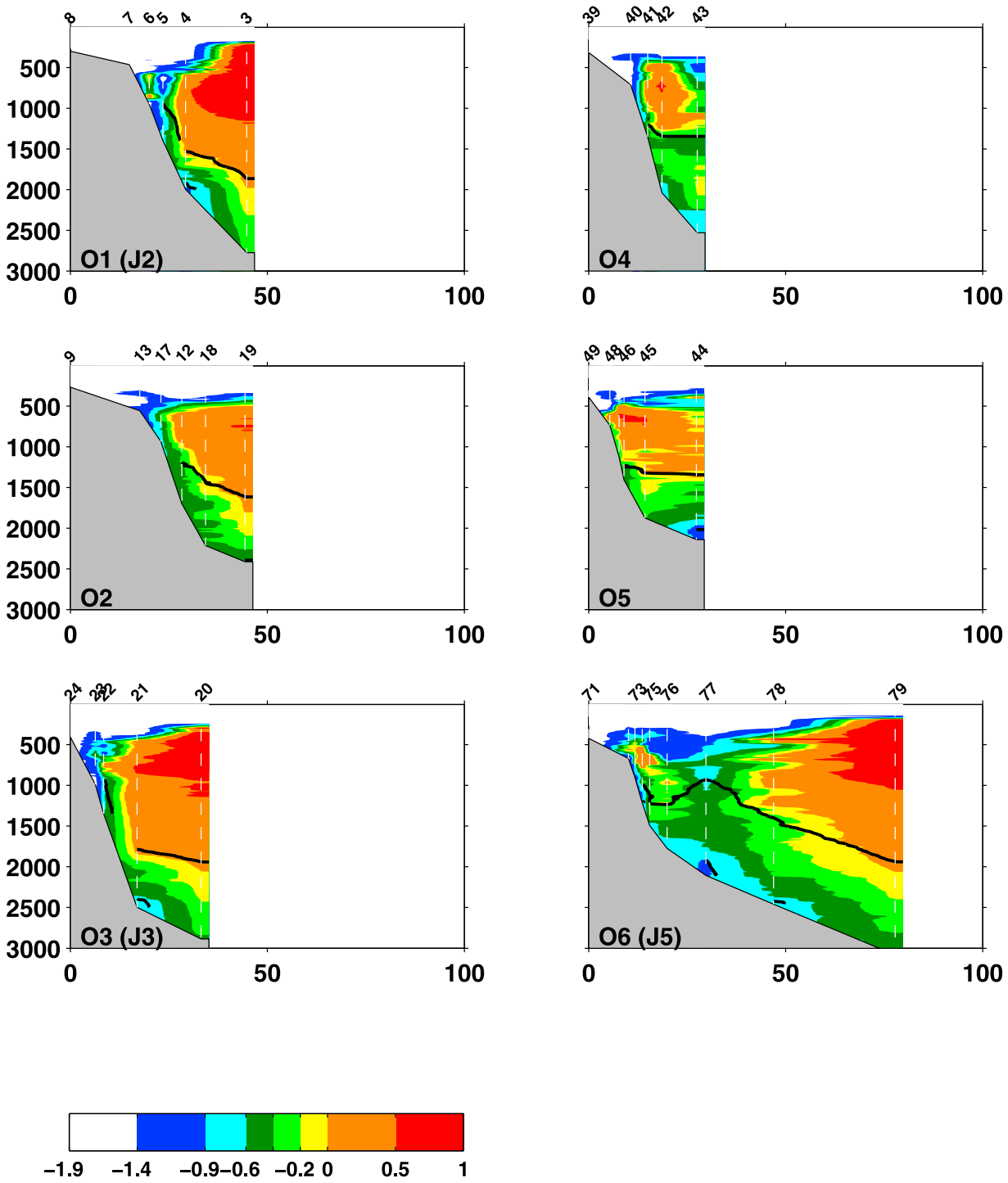

Figure 7. As in Figure 6 but for transects O1–O6 from October 2004 (NBP04–08, Figure 5d). The 0°C isotherm indicating the Antarctic Slope Front is not included.

dense relative to the 28.34 kg m^{-3} contour in $\theta - S$ space. Beginning in the east on transect O1, the ambient AABW signal at station 3 is more saline, warmer and less dense than the bottom layer from nearby summer stations. As in summer, there is evidence of a westward component to the downslope transport from the Mertz source, i.e., through station 4 on O1, station 19 on O2 and station 21 on O3. However, in spring there is also evidence of a more direct northward transport from the Adélie source region at station 71 on transect O6.

[40] While the results above are far from conclusive and the difficulties inherent in observing downslope flows effectively by CTD survey are large, in particular over rough topography, we nonetheless attempt to summarize the broad pattern of the modified shelf water propagation and dual system of AABW formation from the Mertz and Adélie

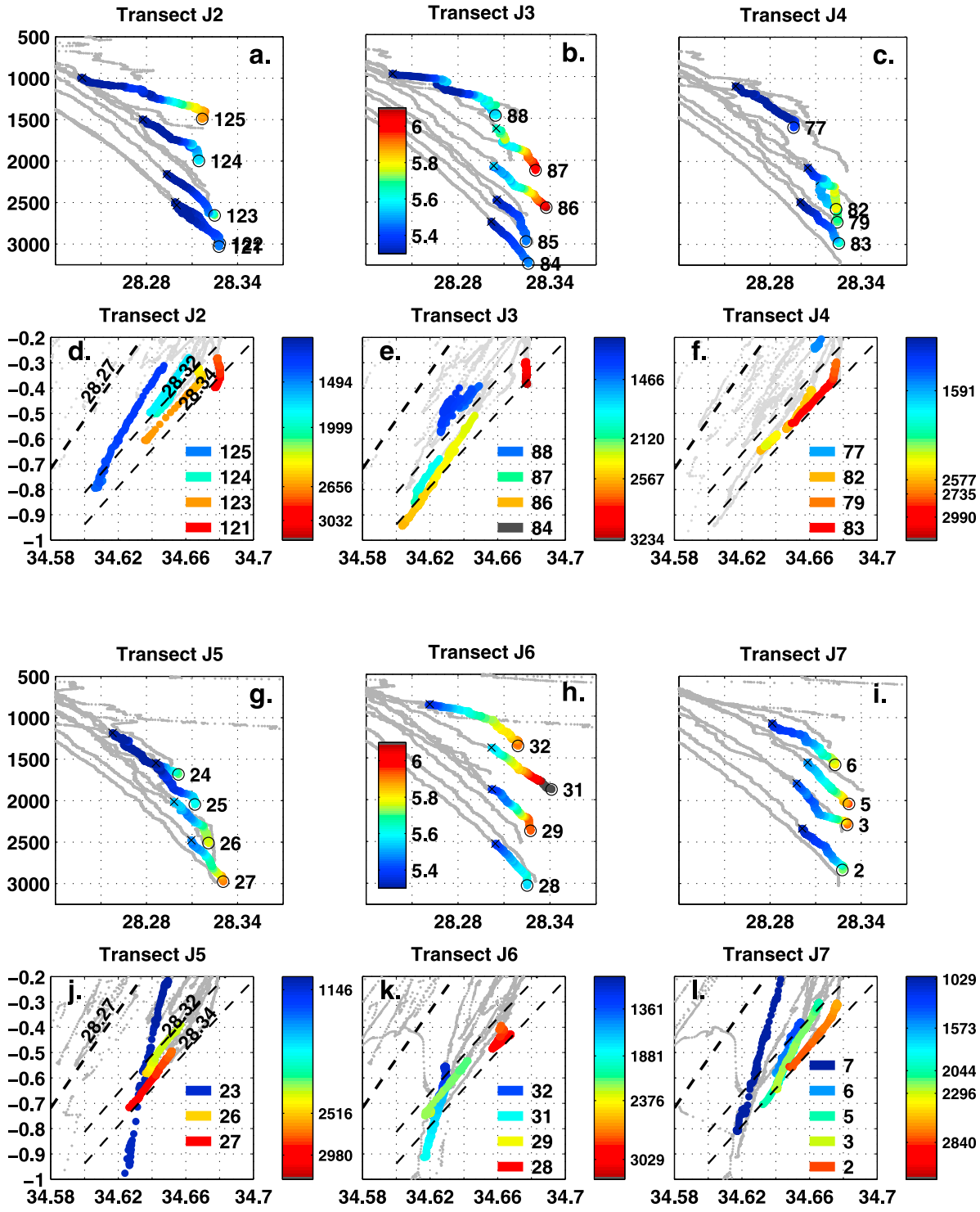

Figure 8. Water mass properties for the bottom 500 m at key stations (greater than 1000 m depth) along transects J2–J7. In each case there are (a–c and g–i) vertical profiles of neutral density (γ_n kg m^{-3}) shaded with dissolved oxygen concentrations (ml l^{-1}) and (d–f and j–l) $\theta - S$ diagrams shaded with depth with γ_n contours shown for 28.27, 28.32, and 28.34 kg m^{-3} as dashed lines. The data from the stations on the preceding transect (to the east) are shaded light gray. Station numbers are as labeled, with the top and bottom of profiles marked with an "x" and "o", respectively.

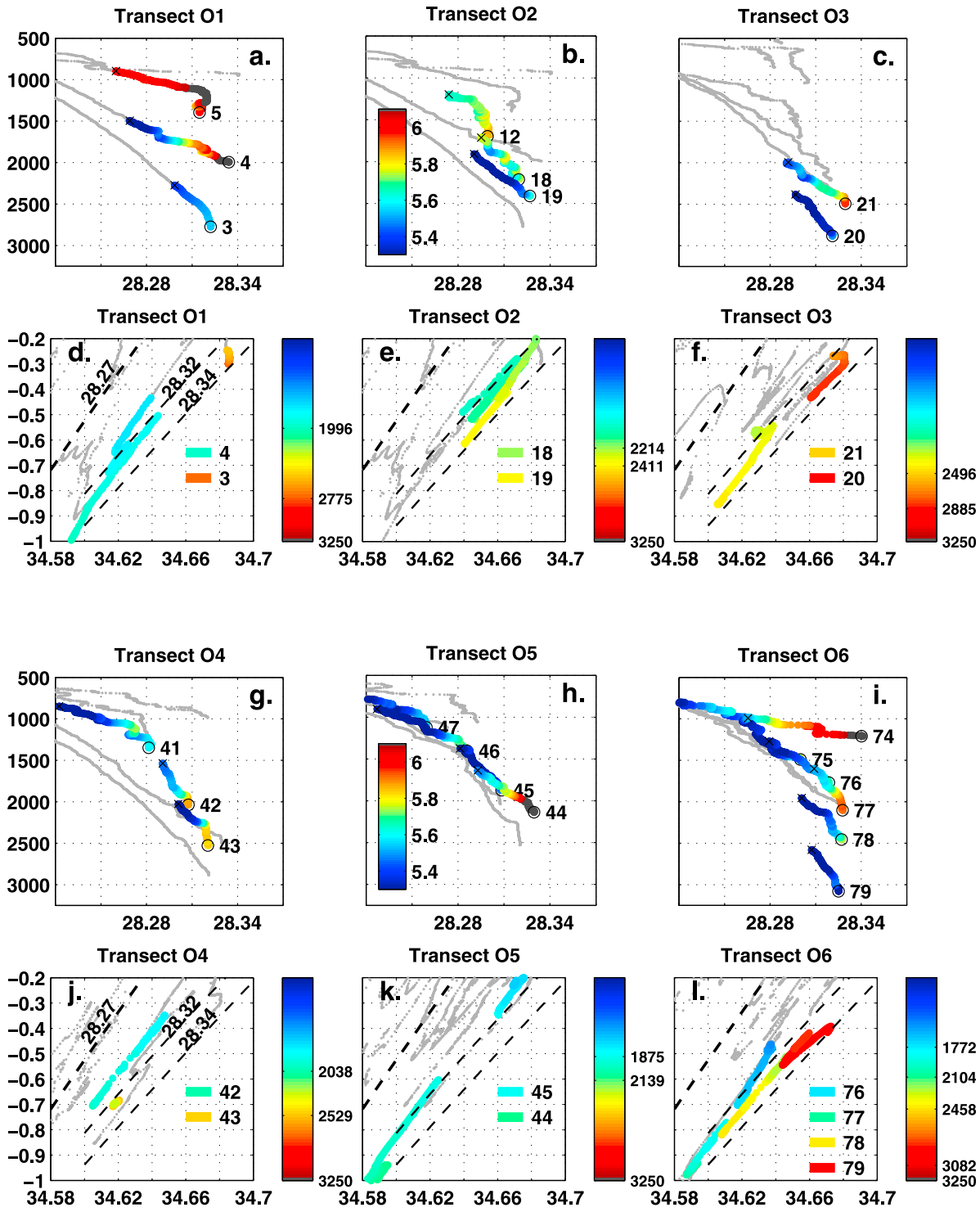

Figure 9. As in Figure 8 but for transects O1–O6 from the NBP04–08 data set.

source regions in Figure 10. The downslope transport from the Mertz source region is initially WNW before topographic steering by the Buffon channel between 144°E and 145°E potentially provides the mechanism for more northerly transport to stations 82, 79 and 83. An potential alternative source for the downslope flow along the Buffon channel is a secondary outflow point from the Adélie Depression through the incision channel "H" makes in the Mertz Bank at approximately 145°E (see section 2.1). Unfortunately this area was not sampled directly by either CTD survey.

[41] We suggest that there are two pathways for dense shelf water to propagate from the Adélie source. The first is

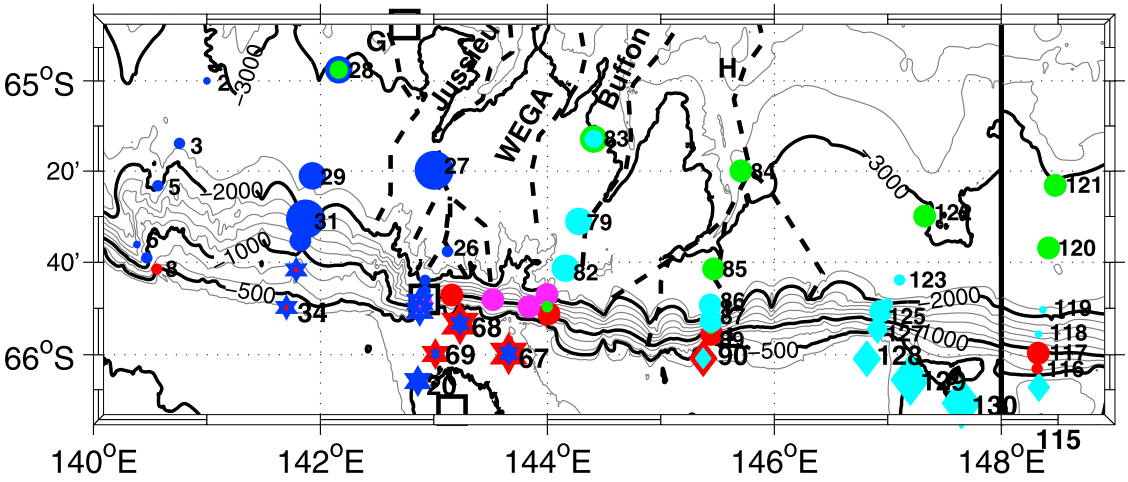

Figure 10a. Bottom layer classification for NBP00–08 data on the continental shelf and slope. Dark and light blue symbols indicate bottom layers with modified shelf water derived from the Adélie Depression (hexagons near shelf break) and Mertz region (diamonds near the shelf break), respectively. Green symbols indicate bottom layers with an ambient AABW signal. Red symbols indicate mCDW intrusions, and magenta symbols indicate the Antarctic Slope Front. The relative strength of bottom layer signatures is roughly denoted by the size of the symbol. Dual-colored symbols depict upper (outer color) and lower (inside color) layering in the bottom layer.

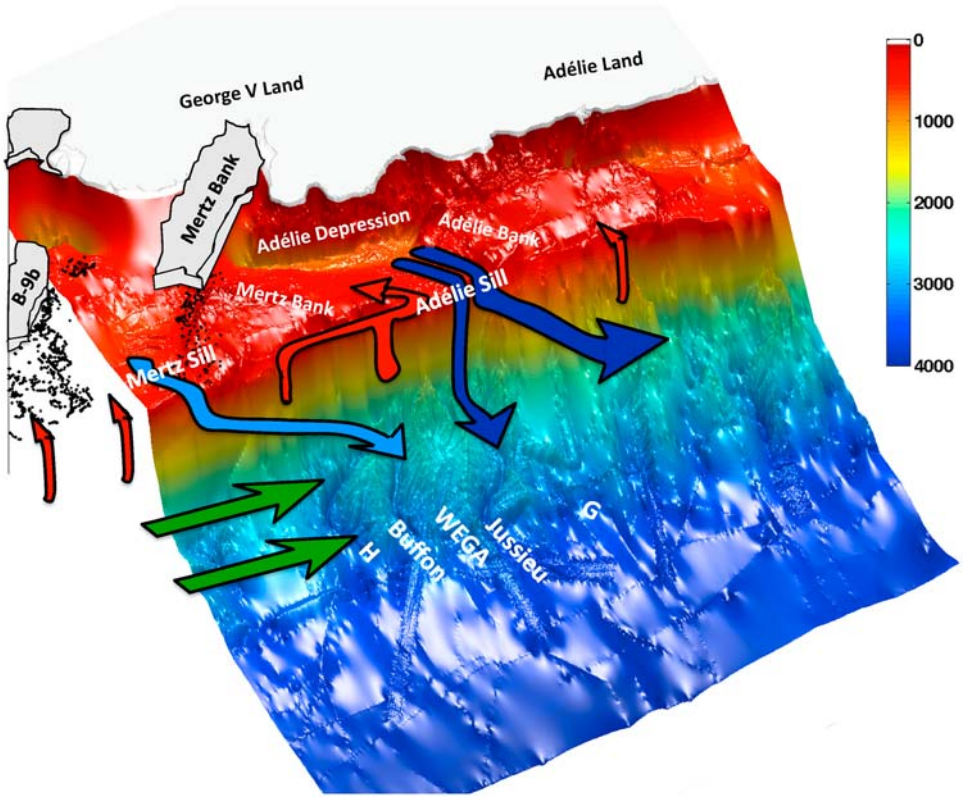

Figure 10b. A 3-D schematic of the dual system of dense shelf water overflows from the Mertz (light blue) and Adélie Depression (dark blue) inferred in this paper. The position of mCDW intrusions near the shelf break and the major pathway of mCDW into the Adélie Depression through the eastern flank of the Adélie Sill is indicated by the red arrows. The westward inflow of ambient AABW is indicated by the green arrows. Bathymetry as in Figure 1a.

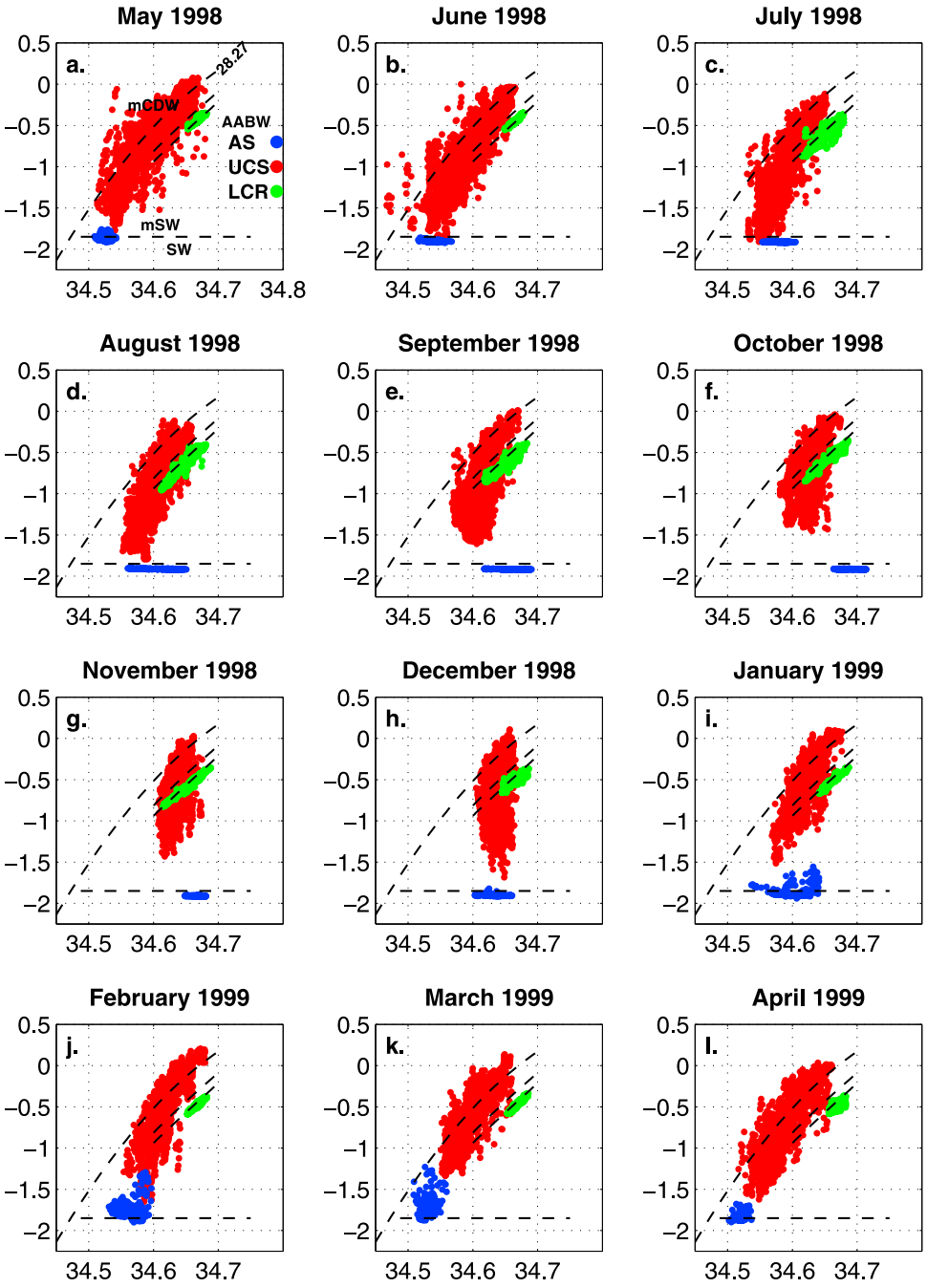

Figure 11. (a–i) Monthly $\theta - S$ diagrams between May 1998 and April 1999 for Microcat data at the Adélie Sill (see Figure 3), Upper Continental Slope (1157 m), and Lower Continental Rise (3196 m). Data colored as shown in Figure 11a. Water masses and boundaries labeled in Figure 11a as in Figure 2. Additional γ_n contours for 28.32 and 28.34 kg m^{-3} are shown for the LCR data.

NW toward the continental rise between 141°E and 142°E, which is most likely to be the pattern observed by the mooring data of *Fukamachi et al.* [2000]. The second is a more direct northward transport down the Jussieu channel near 143°E as observed at station 27 in summer. This latter pathway is the focus of the mooring observations presented in the next section. Figure 10 also indicates the presence of mCDW near the upper slope and shelf break across the region. The major incursion is east of the Adélie Sill with the ASF located just offshore of the shelf break at 144°E. Other areas include east of the Mertz Sill, north of the Mertz Bank near 145.5°E and north of the Adélie Bank near 141°E. That there is an mCDW incursion area immediately east of both the Mertz and Adélie regions is likely due to the conservation of mass compensating for the export of dense shelf water, termed cascade-driven upwelling in modeling studies

by *Kämpf* [2005]. That the strongest mCDW intrusion occurs east of the Adélie source agrees with this being a stronger source of dense shelf water export.

4. Seasonal Production of AABW North of the Adélie Sill

4.1. Monthly $\theta - S$ Properties on the Shelf, Slope, and Rise Along 143°E

[42] We summarize the northward evolution of AABW from the Adélie Depression across all three MPE mooring locations using monthly $\theta - S$ diagrams in Figure 11. At the Adélie Sill (AS), the exported shelf water increases in salinity and density along the surface freezing point line from June to a maximum in October, and then decreases until the following April, leaving the surface freezing point line from December as the presence of warm mCDW increases. At the Upper Continental Slope (UCS) in May, the data are the least dense, parallel with the isopycnals, with the greatest range in potential temperature and salinity. From May through December the data shifts to more saline and cooler values denser than the 28.27 kg m^{-3} isopycnal.

[43] At the cold, fresh extreme of the UCS data, the modified shelf water exhibits a similar and enhanced increase in salinity, but with a warming from July (<−1.7°C) to November (>−1.5°C). In December and February there is some colder, more saline shelf water, but from January through April the background field becomes warmer and fresher and realigned with the isopycnals. The overall pattern here demonstrates the timing of the cold, dense downslope flows, and the seasonal variability of the ambient background field which is unrelated to the local downslope flows here but may be influenced by those upstream from the Mertz Depression.

[44] At the Lower Continental Rise (LCR), the intrusion of new AABW is shown by the increased spread in data from July to January to colder and fresher values. In May and June, the local AABW is warmer than −0.5°C. From July, cold, and fresh AABW appears and persists through November, after which the data returns to the initial state, with weaker and less variable AABW signals (−0.5°–−0.6°) still present from December through March.

4.2. Dense Shelf Water on the Upper Continental Slope North of the Adélie Sill

[45] The data from both Microcats at the UCS mooring site, at 1139 and 1157 m depth, respectively, were so strongly correlated across the entire record that we only show data from the deeper Microcat M-318 (Figures 12a–12c.). The striking feature of the time series at this location relative to the Adélie Sill is the increased short-term variability in the vicinity of the Antarctic Slope Front as the record switches between cold, relatively fresh modified shelf water and warm, saline mCDW. In this location temperature is the dominant component of density, and so the modified shelf water is more dense than the warm and saline ambient field. While this could suggest there is simply a north-south oscillation of the Antarctic Slope Front, we find evidence for the downslope flows in the strong correlation between cold, fresh dense events and the bottom intensified speeds, with $r^2 = 0.8$ for the 2 day mean over the entire record and $r^2 = 0.89$ for August–September period (see Figures 12e–12h.). The 2 day mean speeds from the bottom-mounted upward-looking ADCP are regularly between 20 and 40 cm s^{-1} from July to February with instantaneous values up to 60 cm s^{-1} and a maximum of 80 cm s^{-1} in December. Tidal analysis found the diurnal constituents K1 and O1 contributed 7.3 and 5.3 cm s^{-1}, respectively, and dominated over the longer period constituents.

[46] In Figures 12a–12d we also present the daily range of water mass properties (gray lines) to examine the seasonal cycle of the ambient and shelf water components. In May, the ambient mCDW has salinity greater than 34.65, is close to 0° and dominates over the episodic cold and fresh events that last 3–5 days. Then in June there is a shift to fresher, cooler values. From June to the middle of November the downslope events become more saline and warmer. Over the same period, the mCDW also warmed and became more saline, but the shift is less than observed in the downslope flows. The increase in salinity in the modified shelf water can be explained by the increase in salinity of shelf waters exported through the sill, and while this does not influence the ambient field in this location, downslope flows from the Mertz source upstream could.

[47] However the warming of the modified shelf water is not so easily explained, and appears unrelated to processes on the shelf where the exported water mass is at the near-surface freezing point from May through November. A possible explanation for this is increased influence of mCDW in the depth range 500–1000 m between the Adélie Sill and the UCS moorings. The mCDW would provide both warming and additional salinity to the downslope flow. Regardless of this broad seasonal cycle, it is worth noting that there are still cold and dense events occurring in summer, outside of the peak export season, which suggest some type of seiche-like drainage of the dense shelf water in the Adélie Depression after the dense shelf water returns below the minimum sill depth in summer. An intensification of the local katabatic or even synoptic winds is the likely mechanism for generating the internal wave pattern that could excite such an internal seiche. The closest CTDs collected during both spring (station 74) and summer (station 23) lie within the range of UCS mooring data, though given the variability of the water mass properties at this mooring site it is noted that ship-based CTD observations can easily "hit or miss" the dense shelf water overflows.

4.3. Newly Formed AABW on the Lower Continental Rise Near Channel "G"

[48] The time series of water mass properties from Microcat M-380 at the Lower Continental Rise (LCR) site approximately 160 km north of the Adélie Sill is shown in Figure 13. As indicated previously, this mooring was located on the western flank of the topographic channel labeled Channel "G" by *Carbulotto et al.* [2006]. At the depth of 3250 m the ambient AABW has salinity greater than 34.67 and potential temperature greater than −0.45°C. As observed on the upper continental slope, the newly formed AABW registers as cold, fresh and dense departures from the ambient field. We define three distinct phases in the record, labeled 1, 2, and 3 in Figure 13b.

[49] In phase 1 from May to July 1998 the record is relatively quiescent with evidence of minor downslope flow activity from the very small cold, fresh and dense features

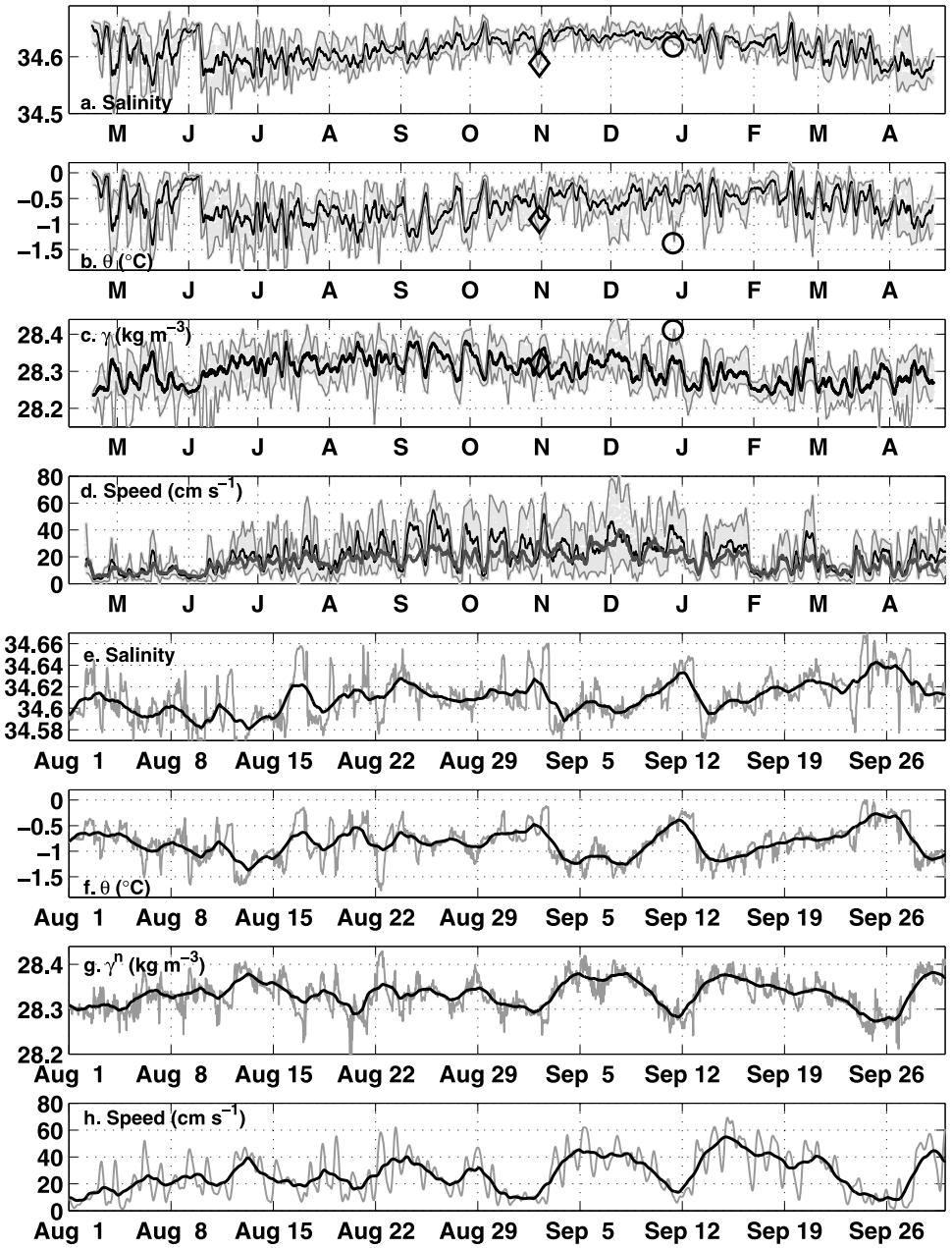

Figure 12. Time series of (a) salinity, (b) potential temperature (°C), (c) neutral density (kg m^{-3}), and (d) ADCP current speed (cm s^{-1}) for Microcat 318 (1157 m) and bottom-mounted upward-looking ADCP (1175m) at the Upper Continental Slope mooring site (1180 m) between April 1998 and April 1999. All data is shown (gray points), bounded by lines of daily minima and maxima (gray), with a 2 day running mean (black line). ADCP data shown for 1154 m and 1050 m (dark gray, running mean only). Nearby CTD data from NBP04–08 (station 74, black diamond) and NBP00–08 (station 23, black circle). (e–h) The data for August through September (gray) with the 2 day running mean (black). ADCP data shown for 1154 m only.

relative to the ambient AABW. In phase 2 from July to the end of November these events are much stronger, with seven of the coldest (−0.8–−0.9 °C) and freshest (34.62–34.63) features occurring from the end of July to the middle of November over time scales ranging between a few days and a fortnight. The salinity change over this period at the Adélie Sill (<34.6 to >34.65) shown in Figures 3 and 11 does not appear at the LCR mooring. This suggests that despite the addition of salinity from the mCDW on the continental slope, the freshening across the outer shelf break and upper slope (locations A–C in Figure 4) dominates. This is in agreement with studies that find the majority of entrainment occurs on the upper slope [*Baines*, 2008]. In phase 3 from December until the end of the record in April 1999 there is

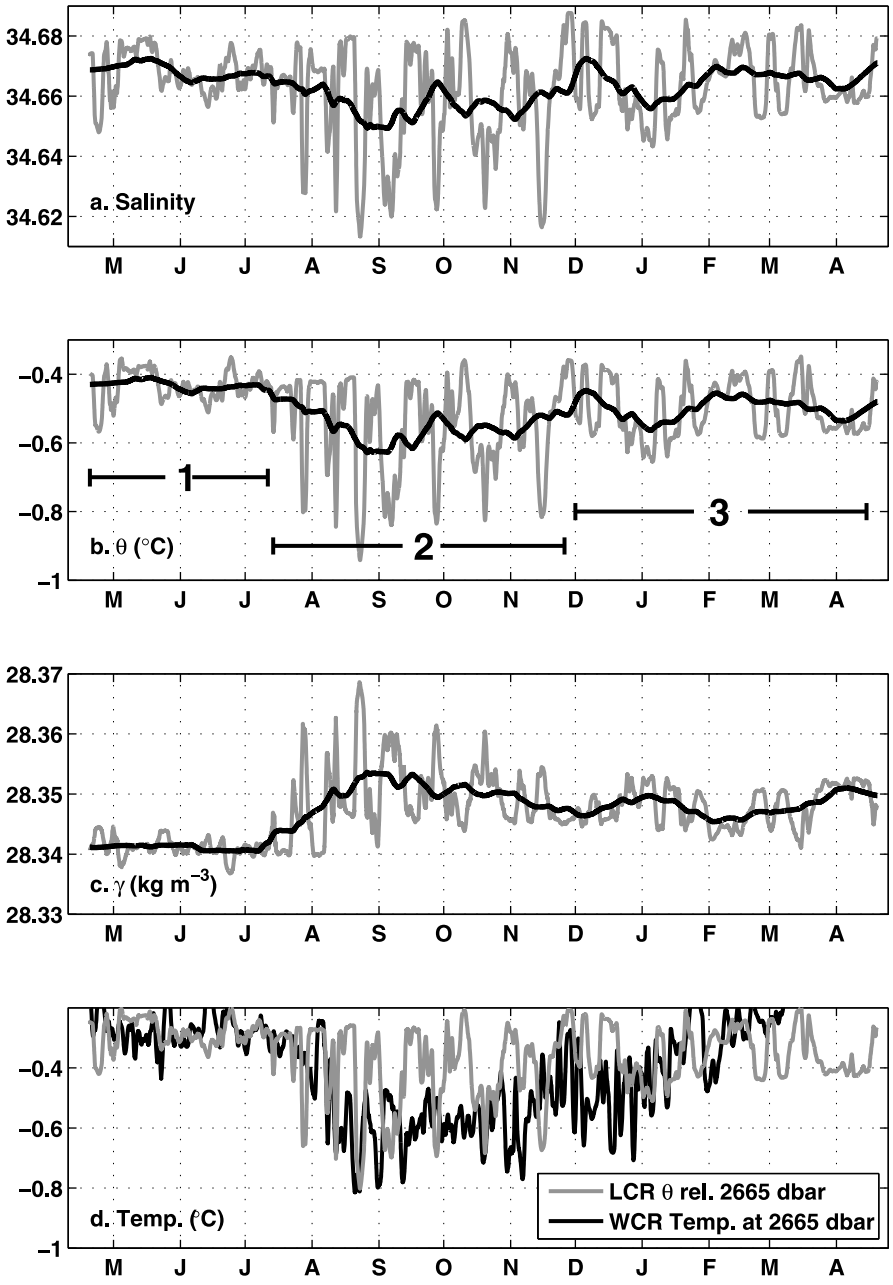

Figure 13. Water mass properties from Microcat 380 at 3196 m at the Lower Continental Rise mooring site in 3213 m ocean depth. (a–c) Salinity, potential temperature (θ°C), and neutral density (γ_n kg m^{-3}). (d) The temperature record from the WCR site at 2665 dbar [*Fukamachi et al.*, 2000] with the LCR potential temperature relative to 2665 dbar. Data shown as 2 day (gray line) and 30 day running mean (black line). Three phases (1, 2, and 3) are labeled as described in the text.

evidence of further downslope flows, though the events are weaker, i.e., warmer (<−0.6°C) and more saline (<34.66) during this period.

[50] We interpret the shift from phase 2 to phase 3 in the time series at the LCR site as the result of seasonal variability in the downslope pathways of AABW from the Adélie Sill. Comparing the LCR temperature record with the temperature record from *Fukamachi et al.* [2000] at the Western Continental Rise (WCR) site, we present their *in situ* temperature data at 2665 dbar with our LCR data as the potential temperature at 3225 dbar relative to 2665 dbar (Figure 13d). Key features of this comparison are: the seasonal variability is relatively similar, there is a similar minimum temperature range but there are more peak events at the WCR mooring relative to the LCR, the episodic nature of the peak events at the LCR site that depart and return to the ambient relative to the broad shift away from the ambient at the WCR location over the same period, and the mean shift

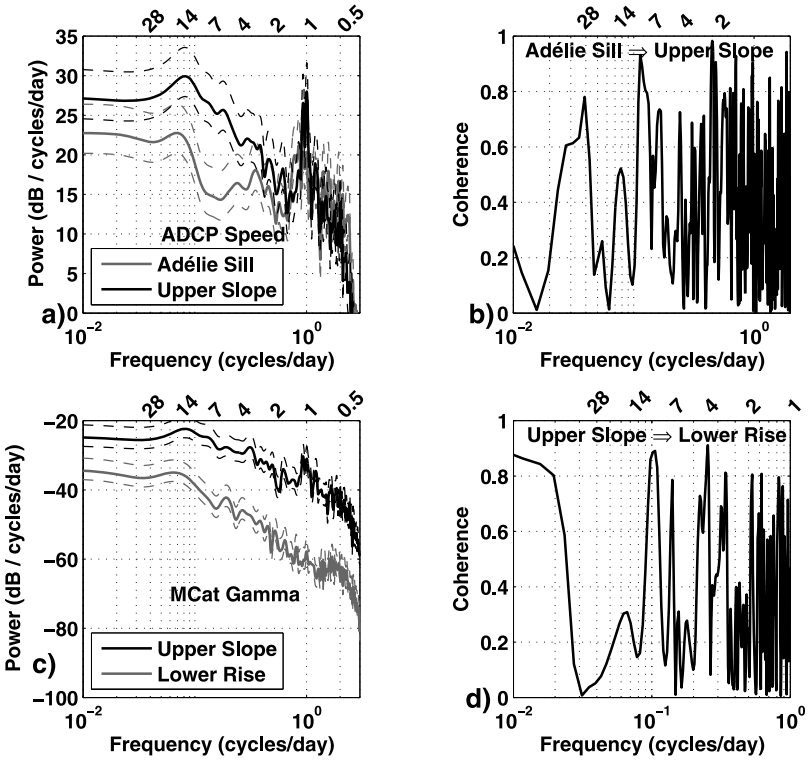

Figure 14. Power spectrum and mean square coherence for the (a and b) ADCP speed record at the Adélie Sill (black line, 454 m) and Upper Slope (gray line, 1157 m) and (c and d) the Microcat neutral density record at the Upper Slope (red line, 1157 m) and Lower Rise (green line, 3196 m). Time period set to phase 2 from July through November 1998 (see Figure 13). Primary abscissa is frequency (cycles day^{-1}), with the period (days) shown above. After prewhitening, a Welch spectral estimator was used with a 50% Hamming window and noverlap = 1024. The power spectral density was calculated using nfft = 8192 and the sampling frequency of 45 min (the microcat data was interpolated onto the ADCP time grid), with the 95% confidence intervals indicated by dashed lines.

to colder values over the period between August and December which is greater by almost 0.2°C at the WCR location.

[51] These suggest that both sites sample the same AABW from the Adélie Sill and the continuous nature of the signal at the WCR site suggests the majority takes this pathway. Modeling studies by *Marsland et al.* [2004] suggest that 1995 had stronger ice formation and dense shelf water export relative to 1998 and this could also contribute to the stronger AABW signal at the WCR site. It is worth noting the LCR mooring site was on the flank of the Channel G, and there may be more continuous downslope flows occurring down its center line that is not accounted for.

[52] The continuation of reduced AABW events during phase 3 has two possible explanations. First, this could be the resulting AABW from the eastern Mertz source region of dense shelf water export, with a seasonal increase in the westward transport. This is unlikely given that the Mertz source is depleted of dense shelf water in summer ahead of the deeper Adélie source. Secondly, these AABW events from December through March could be the lagged advection of AABW from the Ross Sea, which is reported by *Gordon et al.* [2009] to peak from March through May. Given the 1300–1400 km from Cape Adare to the LCR mooring site, and an average westward transport speed of 5–10 cm s^{-1}, the seasonal peak in RSBW in April–May [*Gordon et al.*, 2009] should reach the George V Land region in 10–5 months in summer. However the ambient offshore AABW layer from the NBP00–08 data was warmer than −0.45°E, so this is not the case. Therefore it is most likely that this is simply a continuation of episodic northward transport of dense shelf water from the Adélie Sill, reduced in its cooling and freshening signature by the increased influence of mCDW and AASW over the upper slope during summer seen in Figure 11.

[53] Spectral analysis was conducted on the available time series of speed at the Adélie Sill and Upper Slope (Figure 14a) during July through November (labeled phase 2 in Figure 13) to examine the frequency of downslope events and to assess how "connected" these events were between the mooring locations. Time series had their mean subtracted and were detrended and low-pass filtered (Butterworth with a 9 hr cutoff) before being processed using a Welch spectral estimator (see caption for details). Mean squared coherence between the speed record at the Adélie Sill and Upper Slope is shown in Figure 14b. Comparing the ADCP record, there is significantly more energy on the Upper Slope, with stronger diurnal peaks at the O1 and K1 frequency and weaker semidiurnal peaks relative to the Adélie Sill. Although both signals have peaks in the fortnightly range, the strongest

coherence between the two locations is in the 2–3 day, 9–10 day, and 28 day frequency range.

[54] Similar analysis was carried out on the neutral density record between the Upper Slope and Lower Rise (Figures 14c–14d). There is clearly much less energy in these signals relative to the ADCP record and locations further up the slope. The strong correlation between speed and density at the Upper Slope is reflected in the similar frequency peaks, albeit with damped amplitude in the diurnal and longer period range. The strongest coherence remains in the 9–10 day range, and others in the 3–7 day period (Figure 14d). These periods suggest the influence of weekly to fortnightly synoptic weather patterns on the strongest, northward outflow of dense shelf water and subsequent downslope flow down the topographic channels north of the Adélie Sill (Jussieu and G). Alternatively these "northward" events could be related to instabilities in downslope rotating gravity plumes as shown in theoretical models [e.g., *Swaters*, 2006, 2009a, 2009b].

5. Discussion

5.1. Comparison With AABW Formation in the Western Ross Sea

[55] In broad terms, the mechanisms for AABW formation along the Adélie/George V Land (AGVL) coast and those detailed in the AnSlope studies for the western Ross Sea are similar, in particular when compared to AABW formation in the Weddell Sea [*Foldvik et al.*, 2004]. In both areas there is dense shelf water formation beneath a coastal polynya region enhanced by the blocking effect of a floating glacier tongue. The dense shelf water is subsequently exported across the shelf break, modified through interactions with tides and the Antarctic Slope Front and transported down the continental slope and rise. The similarities even extend to the dual system of high- and low-salinity dense shelf water overflow regions depicted in this paper from the Adélie and Mertz Depressions, respectively, as *Gordon et al.* [2009] describe low-salinity shelf water export through the Joides Trough east of the high-salinity outflow from the Drygalski Trough. However in each of these mechanisms/processes, key differences exist.

[56] In the western Ross Sea, the primary source region for dense shelf water formation is over the deeper part of the Drygalski Trough beneath the Terra Nova Bay polynya north of the Drygalski Ice Tongue on the Victoria Land coast [*Kurtz and Bromwich*, 1985; *Budillon and Spezie*, 2000; *Buffoni et al.*, 2002]. The distance from this formation region to the minimum sill of the Drygalski Trough is over 400km and as a result there is a significant lag in the seasonal cycle of dense shelf water export relative to the formation period. *Gordon et al.* [2009] report that during AnSlope episodic pulses of dense shelf water from the Drygalski Trough peaked in the summer/fall of 2003, with the most extreme events observed from mid-April to mid-May. By contrast the mooring results of this paper and *Williams et al.* [2008] show the dense shelf water export and overflows from the Adélie Depression peaking from July through November.

[57] The most striking feature of the dense shelf water export from the western Ross Sea as revealed by the AnSlope surveys is the intense diurnal tidal currents (over 1 m s^{-1}) and subsequent mixing as the Antarctic Slope Front penetrates inside of the shelf break each day, transporting relatively unmodified CDW as warm and saline as 1°C and >34.7 onto the shelf [*Whitworth III and Orsi*, 2006; *Muench et al.*, 2009; *Padman et al.*, 2009]. A two-dimensional model of the Antarctic Slope Front by *Baines* [2009] found that under steady state conditions the mCDW can only get onto the continental shelf with the assistance of tides. Along the AGVL coast the Antarctic Slope Front remains offshore of the shelf and therefore mCDW incursions are relatively weaker, and almost entirely unidentifiable during the peak winter formation period [*Williams and Bindoff*, 2003]. The shoreward penetration of the ASF reported by *Whitworth III and Orsi* [2006] at mooring locations 17km south of the shelf break is in stark contrast to the observations at the Adélie Sill mooring (reported by *Williams et al.* [2008] and revisited in this paper in Figure 3) which is a comparable distance south of the shelf break but shows only dense shelf water during the peak export months and much weaker semidiurnal and diurnal tidal components (1–2 cm s^{-1}). More prominent mCDW signals, albeit still weaker than in the western Ross Sea are likely to be found to the north and east of the Adélie Sill mooring location presented here.

[58] The dense shelf water exported from the Drygalski Trough is much more saline (34.75–34.8) than along the AGVL coast and mixes more with warm, saline mCDW than the cool, fresh AASW across the ASF region. The density dependency of overflows appears to switch from salinity (Ross) to temperature along the AGVL region. This implies that thermobaricity, i.e., the increased influence of temperature on density with depth, may be more important for overflows along the AGVL and assist the relatively fresher shelf water to become AABW, as proposed by *Gordon et al.* [2009] for the cold and fresher low-salinity shelf water exported from the Joides Trough in the Ross Sea. Whereas *Muench et al.* [2009] identify the bottom layer from a transition to cold and saline properties in $\theta - S$ properties, the AGVL bottom layer is marked by cold and fresh properties. This may be due to the increased influence of mCDW across the ASF in the Ross Sea, whereas in the AGVL region the bottom layer initially loses salinity through mixing with AASW near the shelf break south of the ASF and then gains salinity through further entrainment of UCDW downslope, but ultimately decreasing in density through warming. Clearly the timing and nature of AABW formation processes differ between the two regions and therefore care must be taken to simulate these differences in modeling studies that seek to cover both regions.

[59] In laboratory experiments, *Baines* [2008] divided downslope flows into stratified environments into two categories: detraining gravity currents on sufficiently gentle slopes (up to 12°) and entraining plumes on sufficiently steep slopes (greater than 30°). Furthermore, he presented a criterion for gravity currents whereby the bottom drag coefficient and minimal entrainment must be sufficient to balance the buoyancy force acting on the flow and determined that although the slope angle for the downslope flows north of the western Ross Sea was gentle enough to be considered a gravity current, the amount of observed entrainment [*Gordon et al.*, 2004; *Muench et al.*, 2009; *Gordon et al.*, 2009] violated this criterion and therefore he labeled this flow an entraining plume. Given the bottom drag coefficient is much smaller in the ocean than it is in the laboratory,

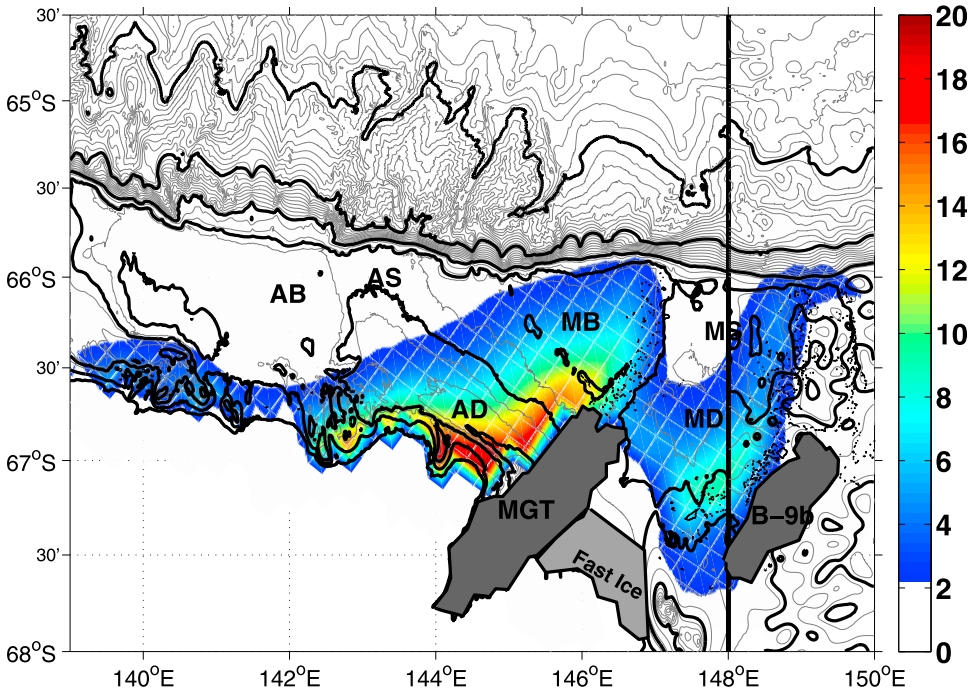

Figure 15a. Mean annual sea ice production rates (m m^{-2}) over the Adélie Depression and surrounding regions between 1992 and 2001 from the ERA40 data product [*Tamura et al.*, 2008].

entraining plumes in the ocean should occur at much smaller slope angles. Similarly the maximum slope angles along the AGVL coast do not exceed 11° but there is a general thickening of dense shelf water overflows with depth (for more detail see Tables A1 and A2 in Appendix A) and so it is likely the same entraining plume model applies there too.

5.2. Ice Production Over the Mertz Depression and Mertz Bank

[60] The key finding from the CTD observations presented in this paper is the identification of dense shelf water overflows on the continental slope between 144°E and 148°E originating as relatively low-salinity dense shelf water from

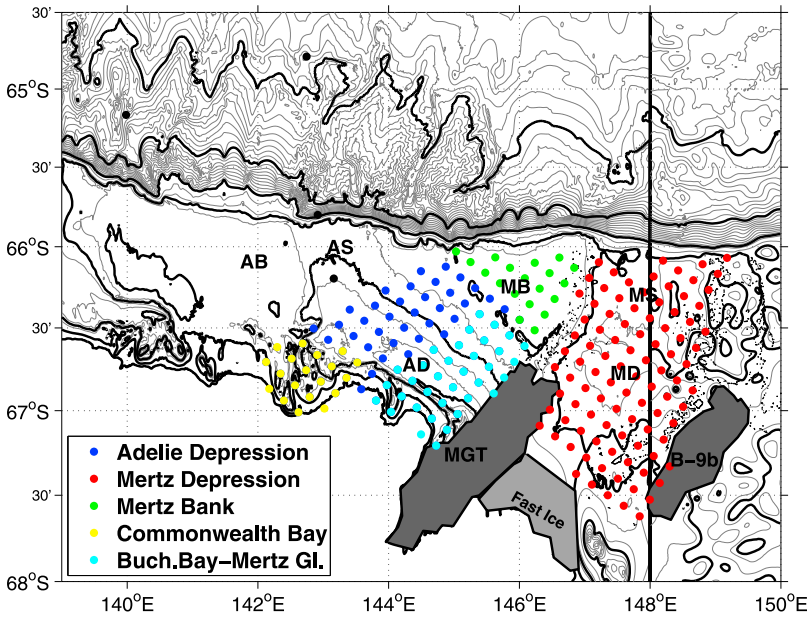

Figure 15b. Data masks for regional polynya areas. The Adélie Depression mask (blue lines) includes subregions against the Mertz Glacier (cyan) and in Commonwealth Bay (yellow). Ice production over the Mertz Bank (green) and Mertz Depression is independent of the Adélie Depression.

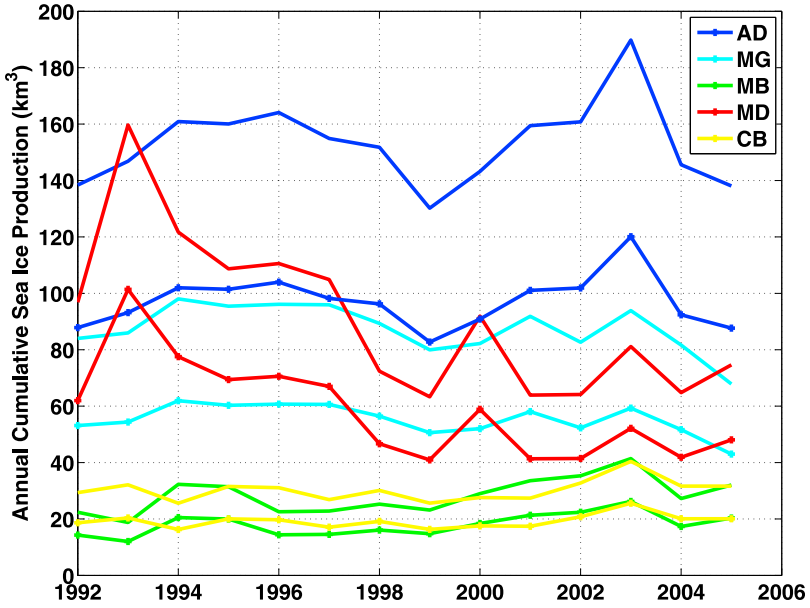

Figure 15c. Total annual sea ice production (km^3) with upper (NCEP-2 data from 1992 to 2005; upper thick lines) and lower bounds (NCEP-2 data from 1992 to 2005 with the mean offset from ERA40 between 1992 and 2001; thick lines with boxes). Colors indicate polynya regions shown in Figure 15b.

the Mertz Depression (see Figures 5c and 10). To investigate this source region further and its potential contribution to the total dense shelf water export for the AGVL coast we use mean annual sea ice production estimates from satellite data between 1992 and 2001 [*Tamura et al.*, 2007, 2008]. Figure 15 describes the ice production in the regional polynya areas west and east of the Mertz Glacier Tongue. While the primary polynya regions within the Adélie Depression both have a maximum 20 m m^{-2} of ice production, Figure 15a demonstrates that there are two other additional regions, namely the Mertz Depression east of the Mertz Glacier Tongue, and the extended shelf break north of the Mertz Bank, that produce up to 10 and 5 m m^{-2}, respectively. This analysis was extended as far as 160°E and found no other significant ice production regions (not shown).

[61] We propose that during the active sea ice formation period both regions produce dense shelf water overflows resulting in local AABW formation, i.e., both regions have enhanced sea ice production, are assumed to be bathymetrically independent (although *Domack and Anderson* [1983] suggest the Adélie Depression extends beneath the MGT to the eastern region and grounding line of the Ninnis Glacier south of the Ninnis Bank) and have access to the continental slope. The CTD data from both spring and summer does not conclusively confirm an export location of dense shelf water formed beneath these regions, but does show dense shelf water on the western side of the Mertz Sill and on the Mertz Bank. It is likely that these areas are connected beneath the fast ice region that forms around the grounded icebergs at the northern tip of the MGT, and so dense water from the Mertz Depression could flow directly out of the Mertz Sill, or west beneath the fast ice and through the grounded icebergs and receive additional brine rejection north of the Mertz Bank before departing the shelf.

[62] The relative strength of these regions, and their interannual variability over the period 1992–2005 is examined in Figures 15b and 15c. Mean sea ice volume over the Adélie Depression is 125 km^3, with small interannual variability relative to the mean production over the Mertz Depression which has 95 km^3 between 1992 and 1997 and 59 km^3 between 1998 and 2005. Together with the production over the Mertz Bank, this represents up to 90% and 70% of the Adélie Depression contribution, respectively, and confirms that a significant amount of brine rejection and shelf water densification occurs outside of the Adélie Depression.

[63] Icebergs can assist or block polynya formation depending on their position relative to the prevailing winds and the local advection of sea ice. In the western Ross Sea, the presence of the large iceberg C-17 over the Drygalski Trough is credited with a decrease in the export of high-salinity shelf water in 2004 relative to 2003 [*Gordon et al.*, 2009]. There are no icebergs in the Adélie Depression and the ice production is relatively consistent. However there are several medium sized icebergs on the eastern side of the Mertz Glacier during the 1990s that regularly changed positions and eventually left the region in 2002 [*Massom*, 2003]. This is the most likely cause of the decreasing ice production in this region, though we note that the decline begins several years before the major icebergs departed.

[64] We note that in the work of *Tamura et al.* [2008], the ice production east of the Mertz Glacier was not included in the total for the Mertz Glacier polynya region (~120 km^3). This decision was made to facilitate comparison with model estimates of ice production that did not capture the additional polynya region east of the Mertz Glacier, such as in the work of *Marsland et al.* [2004]. The total contribution of both regions (~120 + 60 km^3) is now therefore equivalent to

the total estimated for the Cape Darnely polynya (180 km^3) [*Tamura et al.*, 2008]. It is recommended that future modeling studies of this region use the combined total for the AGVL region and simulate both polynya regions either side of the Mertz Glacier.

5.3. A Critical Shelf Water Density for AABW Formation

[65] The concurrent mooring observations presented in this paper tracking dense shelf water export via the topographic channels north of the Adélie Sill invites a reexamination of the minimum density necessary for local AABW formation. A misperception resulting from the density range shared by AABW and shelf water, i.e., $\gamma^n > 28.27$ kg m^{-3} is that this is also the minimum density for AABW formation. Were this the case, shelf water with salinity as low as 34.47 (see Figure 2 inset) would form AABW. However as demonstrated in section 3, the entrainment of warm and saline mCDW results in a net decrease in the density of AABW relative to the shelf water it originated from. That is, shelf water must be significantly greater than $\gamma^n > 28.27$ kg m^{-3} to reach that isopycnal depth offshore.

[66] Previously *Bindoff et al.* [2001] used a simple two end-member mixing line extrapolated from the cold, fresh local AABW end member in $\theta - S$ space to the distribution of shelf water along the near-surface freezing line and determined that the minimum requirement for AABW formation from the Adélie Depression was salinity of at least 34.63, or $\sigma_\theta > 27.88$ kg m^{-3}. *Williams* [2004] demonstrated with a simple kinematic stream tube model fitted to the MPE mooring and NBP00–08 CTD observations on the continental slope that the true mixing path in $\theta - S$ space was curved assuming that the downslope event entrained ambient water mass properties that varied with depth, and found shelf water with $\sigma_\theta > 27.85$ kg m^{-3} was dense enough to form AABW. Accordingly, *Williams et al.* [2008] used both values to set upper and lower bounds on an estimate of dense shelf water export from the Adélie Depression.

[67] We now revisit the estimate of the critical density of shelf water required to produce AABW from the Adélie Depression by examining the offshore mooring observations presented earlier. Peak northward production of AABW (labeled phase 2 in Figure 9) begins in July when the potential density (σ_0) of exported shelf water in the Adélie Sill is no less than 27.85 kg m^{-3}. The expected lag between the two mooring locations is in the order of 5–10 days at a mean speed of 40–20 cm s^{-1} and therefore negligible in this assessment. While the peak period of northward transport from the Adélie Sill finishes at the end of November, weaker AABW signals continue to be detected at the northern LCR moorings site and the western WCR mooring site until February. This agrees with the potential density of exported shelf water remaining greater than 27.85 kg m^{-3}.

[68] However, we note that the low-salinity dense shelf water on the western side of the Mertz Sill attributed to the overflows observed between 145°E and 146°E in summertime is between 27.8 and 27.82 kg m^{-3} at stations 129 and 130. This implies that the minimum density for downslope flows from the eastern Mertz source region is less than the Adélie Depression. There are two factors that could influence this. First, as introduced in section 2, the upper continental slope is steeper offshore from the eastern source relative to north of the Adélie Depression and as slope angle in this depth range is one of the critical factors in downslope flows [*Baines*, 2008] then this may assist less dense shelf water in mixing downslope with less modification. We note that in section 3, the bottom layer at stations attributed to the eastern source appear to be less modified than those downstream of the Adélie source. Secondly dense shelf water overflows can be expected to increase the density of the downstream ambient field, i.e., the downslope flows from the Mertz source increase the density of the ambient field for the Adélie source, as indicated by the seasonal cycle of the UCS mooring from June to October in Figure 12. If the ambient field becomes denser, then this should raise the threshold for negative buoyancy from the Adélie overflow.

[69] Overall the errors and assumptions associated with the estimate of dense shelf water export from different observation platforms in different regions are not insignificant and care is needed when evaluating them, in particular with respect to the strong interannual variability that has been reported by modeling studies [*Marsland et al.*, 2004; *Assmann and Timmermann*, 2005]. At the same time, modeling studies seeking a fixed minimum density criterion for AABW formation need to take into account the variability of this value between regions, and as shown above, within regions that have dual sources. Ultimately, given the rapid changes occurring in all regions and water masses associated with AABW formation, relying on fixed water mass definitions and critical densities for AABW formation is problematic when trying to assess long-term variability and change.

5.4. AABW From Other East Antarctic Polynyas in the Australian-Antarctic Basin Sector

[70] The ice production estimate of ~60 km^3 places the additional eastern Mertz source region on par with other minor polynya regions around the Australian-Antarctic Basin sector of East Antarctica, i.e., the Dibble, Dalton, Vincennes, Shackleton and Barrier polynyas. Of these, only the Dalton has less ice production capacity (Table 1) [*Tamura et al.*, 2008]. If the Mertz Depression polynya initiates the downslope flows on the George V Land slope observed in this paper, then there may be speculation that these other regions also have the capacity to form AABW. However there is little evidence to support this in the water mass properties of the bottom layer between 90°E and 140°E in summertime. Bottom values of CFC-11 concentrations measured during the "BROKE" survey in January–March 1996 were critical in attributing local AABW formation to the AGVL coast and are presented for the first time here in Figure 16a to identify any other AABW formation sites. While the meridional transects do not exactly align with each of the East Antarctic polynyas, there is qualitative evidence of small maxima in bottom concentrations west of the Dibble Glacier, and to a lesser extent the Dalton Ice berg Tongue. A broad northwestward downslope transport from these sources is shown in Figure 16b with no additional near-surface water found at the bottom west of 110°E.

[71] Of course dense shelf water export requires more than just brine rejection from ice production. One theory resulting from the apparent dominance of the AGVL region is that

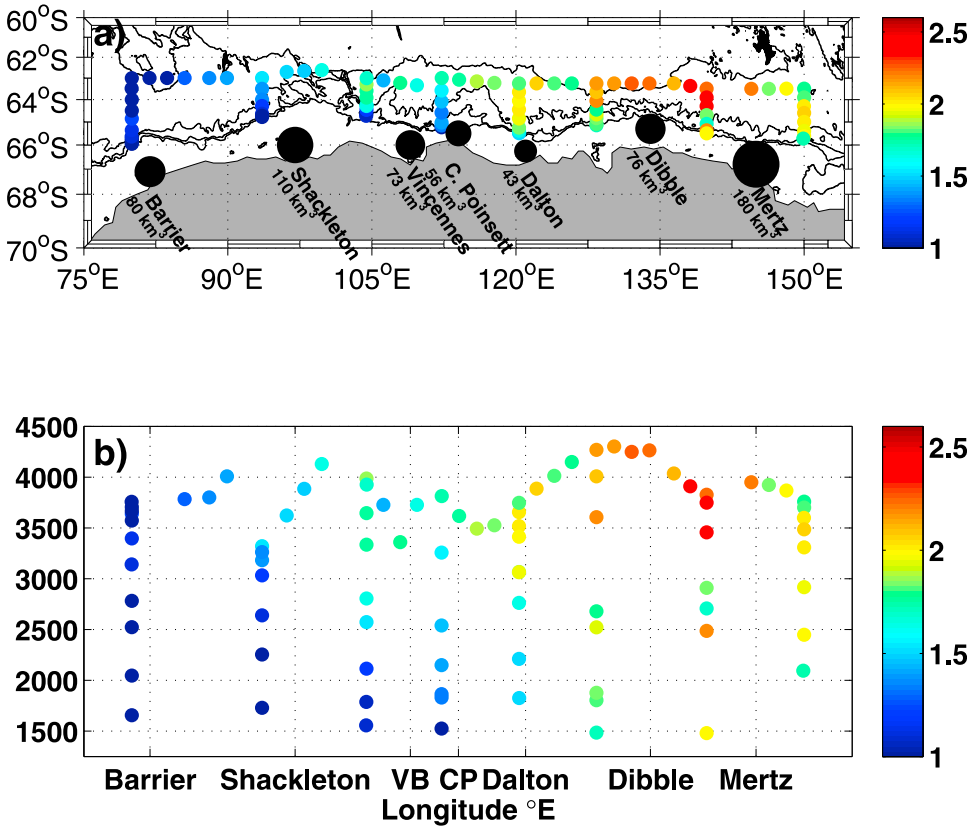

Figure 16. (a) Bottom CFC-11 concentrations (pmol kg^{-1}) at CTD stations greater than 1500 dbar depth from the BROKE survey in January–March 1996 (color scale as shown). The major East Antarctic polynyas are as labeled with mean annual ice volume production (1992–2001) from *Tamura et al.* [2008] as filled black circles with the exception of the Mertz estimate which is from this paper, including ice production over the Mertz Depression, and the Cape Poinsett estimate which is from ERA-Interim data between 1992 and 2006 (not shown). (b) Data from upper panel presented for depth versus longitude.

polynya regions where brine rejection occurs near the shelf break and/or lack a suitable continental shelf depression for the storage of dense shelf water before export have been dismissed as candidates for AABW formation. This idea is to be tested from forthcoming observations from the Cape Darnley polynya region conducted during the International Polar Year. The shelf region beneath the Cape Darnley polynya region is relatively narrow and has only small, shallow depressions. Should the Cape Darnley polynya region prove capable of significant dense shelf water export, then the case for additional AABW formation from other narrow shelf regions with low storage capacity will increase, in particular during the winter sea ice formation period. While their individual input to global AABW volumes is likely to be small, combined there could be a significant contribution to the total AABW production of this region and the rapid changes that have been detected in the last 50 years. There is also renewed interest in the southward transport of mCDW onto the continental shelf that is synonymous with the northward transport of dense shelf water, for biological (krill larvae transport), physical (increased heat flux to ice sheets) and biogeochemical (aragonite saturation horizons) reasons. Therefore future work should address all East Antarctic dense shelf water overflow sites together.

6. Conclusion

[72] This paper presents observations of the downslope transport of dense shelf water on the Adélie and George V Land continental shelf break, slope and rise between 140°E and 149°E from mooring and CTD measurements. The key finding from the CTD observations in summer and spring was the detection of an additional region of dense shelf water overflow, east of the known export region across the Adélie Sill, thus describing a dual system of AABW formation in this region. Modified shelf water and AABW on the slope and rise east of 147°E originates from a lower-salinity form of dense shelf observed on the western flank of the Mertz Sill. This is sourced from ice production in the polynyas over the Mertz Depression (~60 km^3 yr^{-1}), with potential assistance from the polynya over the Mertz Bank (~20 km^3 yr^{-1}) in the lee of the grounded icebergs at the northern end of the Mertz Glacier Tongue. The additional source region makes the total ice production west and east of the Mertz Glacier in the order of ~180 km^3 yr^{-1}. The shelf

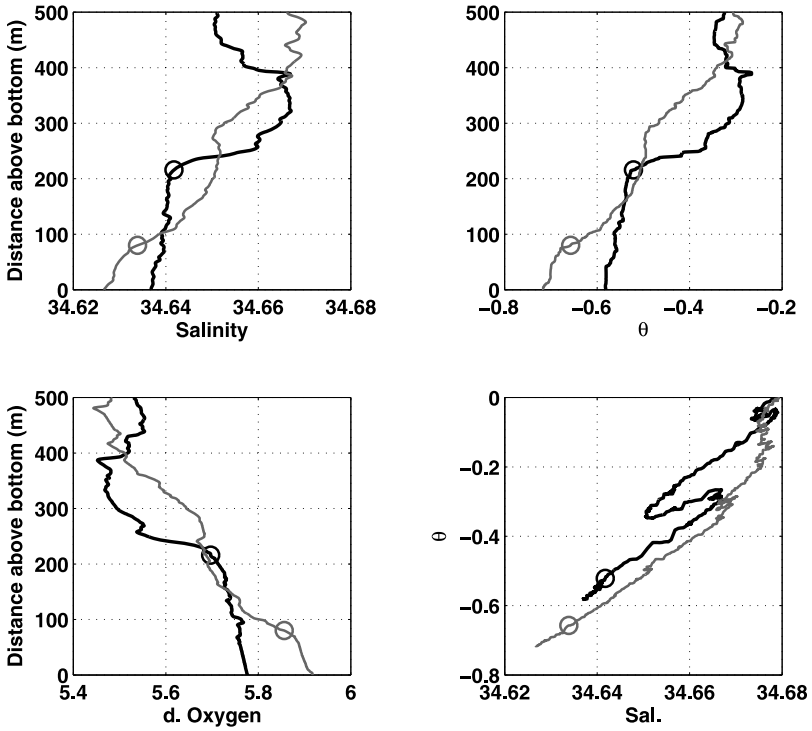

Figure A1. Two examples of bottom layer thickness (H_b, open circles) selection for CTD stations in Tables A1 and A2.

water from the eastern Mertz source with density as low as 27.8–27.82 kg m^{-3} appears capable of producing downslope flows and implies that previous estimates of dense shelf water export in relation to AABW production from the region may have been conservative.

[73] Concurrent time series of Microcat and ADCP data from April 1998 to April 1999 describe for the first time the seasonal variability of the dense shelf water overflows from the Adélie Depression on the upper continental slope and lower continental rise north of the Adélie Sill export region. On the upper slope there was increased diurnal tidal forcing relative to the Adélie Sill export region and a clear oscillation between cold and fresh modified shelf water and warm and saline modified Circumpolar Deep Water in the vicinity of the Antarctic Slope Front. The modified shelf water correlated strongly with increased bottom speed record by ADCP (up to 60 cm s^{-1}) and are assumed to be flowing downslope. On the lower slope in the vicinity of Channel "G," newly formed AABW that was colder, fresher and denser than the ambient AABW was detected throughout the year. The strongest AABW signal was between July and November, with weaker AABW signals continuing through until the following April. Previous mooring data at 140°E suggested a northwestward transport pathway of AABW from the Adélie Depression. These results show there is an additional pathway to the north assisted by the topographic channels. The concurrent observations from shelf to rise suggest the minimum shelf water density for AABW formation north of the Adélie Sill is 27.85 kg m^{-3}.

[74] Several limitations and sources of error are present in this study, in particular the inadequate compass on the moored ADCP instruments and the quality of data from near bottom Microcats near turbidity currents. It is also inherently difficult to observe the time-evolving three-dimensional structure of downslope flows over complex bathymetry with rough bottom topography. It is hoped that upcoming results from subsequent mooring deployments and ship-based surveys in the AGVL region from the Climate of Antarctic and Southern Ocean (CASO) and Adélie Land Bottom water and Ice Ocean iNteraction (ALBION) projects, with improved ADCP compass and range capabilities, will extend the dynamical understanding of the processes described here. The complex nature of downslope flows around the East Antarctic margin presents an ongoing challenge to both the observing and modeling communities attempting to monitor long-term AABW production and its response to climate change scenarios. While satellites are now monitoring the sea ice production in multiple polynya regions around Antarctica and high-resolution ocean ice models are simulating the dense shelf water formation and export from these locations, further work is still required to satisfactorily resolve the final volume transport of AABW after downslope mixing in coupled global models.

[75] **Note added in proof.** During the final stages of publication for this manuscript there were some dramatic changes to the ice front of the George V Land region that are directly related to our findings and worthy of brief discussion here. In January 2010 the B9b iceberg became 'ungrounded', migrating south and ultimately colliding with the MGT on the 12–13th February, calving a new iceberg (C28) that represents almost half of the glacier (http://www.aad.gov.au/MediaLibrary/asset/MediaItems/ml_402353967939815_Mertz_FINAL_100226.pdf).

[76] As detailed in this paper, the previous configuration of both the MGT and B9b promoted dense shelf water

Table A1. Bottom Layer Properties for NBP00—08 CTD Stations With Modified Shelf Water/AABW[a]

Station	Depth	Longitude	q_b (°C)	S_b	dO_b (ml l^{-1})	γ_b (kg m^{-3})	H_b (m)	q_h (°C)	S_h	O_h (ml l^{-1})	γ_h (kg m^{-3})
118	1605	148.33	−0.57	34.636	5.64	28.328	55	−0.37	34.652	5.48	28.312
119	2297	148.37	−0.47	34.649	5.58	28.331	87	−0.39	34.660	5.49	28.327
120	2538	148.42	−0.43	34.659	5.53	28.335	158	−0.42	34.660	5.52	28.334
121	3032	148.48	−0.40	34.677	5.46	28.344	132	−0.40	34.678	5.46	28.344
125	1494	146.93	−0.76	34.609	5.88	28.329	94	−0.77	34.609	5.88	28.330
124	1999	146.99	−0.49	34.642	5.59	28.326	149	−0.47	34.647	5.55	28.325
123	2656	147.10	−0.61	34.635	5.73	28.340	26	−0.59	34.638	5.70	28.339
122	2996	147.32	−0.39	34.679	5.46	28.344	56	−0.39	34.680	5.45	28.344
88	1466	145.44	−0.48	34.637	5.60	28.313	241	−0.47	34.637	5.59	28.307
87	2120	145.44	−0.85	34.611	5.99	28.347	220	−0.82	34.613	5.96	28.344
86	2567	145.44	−0.94	34.604	6.10	28.357	317	−0.70	34.628	5.84	28.343
85	2971	145.47	−0.37	34.676	5.47	28.339	111	−0.37	34.678	5.46	28.339
84	3234	145.71	−0.38	34.676	5.49	28.341	74	−0.38	34.677	5.48	28.340
77	1591	144.00	−0.24	34.662	5.41	28.300	91	−0.24	34.664	5.40	28.301
82	2577	144.16	−0.64	34.631	5.81	28.337	277	−0.61	34.636	5.77	28.337
79	2735	144.28	−0.55	34.647	5.71	28.339	205	−0.55	34.647	5.70	28.339
83	2990	144.41	−0.54	34.649	5.68	28.341	10	−0.54	34.650	5.67	28.341
23	1146	142.88	−1.40	34.617	6.78	28.414	96	−0.99	34.625	6.34	28.369
24	1687	142.92	−0.44	34.637	5.72	28.308	37	−0.43	34.639	5.70	28.307
25	2049	142.92	−0.44	34.649	5.62	28.323	69	−0.43	34.650	5.61	28.322
26	2516	143.12	−0.58	34.636	5.78	28.335	216	−0.56	34.639	5.75	28.332
27	2980	143.00	−0.72	34.627	5.92	28.347	80	−0.70	34.630	5.89	28.347
32	1361	141.82	−0.67	34.625	5.91	28.332	311	−0.60	34.628	5.83	28.322
31	1881	141.87	−0.91	34.616	6.21	28.362	231	−0.80	34.622	6.06	28.349
29	2376	141.93	−0.74	34.619	5.93	28.343	176	−0.73	34.620	5.93	28.342
28	3029	142.16	−0.43	34.667	5.56	28.340	104	−0.43	34.667	5.56	28.340
7	1029	140.47	−0.81	34.616	6.13	28.344	104	−0.70	34.622	5.99	28.332
6	1573	140.38	−0.58	34.640	5.82	28.337	103	−0.56	34.642	5.78	28.335
5	2044	140.57	−0.70	34.632	5.96	28.349	119	−0.62	34.641	5.86	28.345
3	2296	140.76	−0.64	34.640	5.93	28.348	46	−0.64	34.641	5.91	28.348
2	2840	141.00	−0.56	34.648	5.72	28.343	60	−0.55	34.650	5.71	28.344

[a]Subscript "b" denotes bottom values and "h" denotes the mean across the bottom layer thickness H_b, following *Muench et al.* [2009].

Table A2. As in Table A1 but for NBP04—08 in October 2004

Station	Depth	Longitude	q_b (°C)	S_b	O_b (ml l^{-1})	γ_b (kg m^{-3})	H_b (m)	q_h (°C)	S_h	O_h (ml l^{-1})	γ_h (kg m^{-3})
5	1398	147.26	−0.70	34.617	5.98	28.326	68	−0.71	34.617	6.00	28.327
4	1997	147.34	−0.98	34.593	6.24	28.351	117	−0.83	34.607	6.10	28.342
3	2776	147.30	−0.30	34.685	5.53	28.336	46	−0.30	34.685	5.54	28.336
15	852	146.27	−0.81	34.586	6.14	28.284	227	−0.79	34.587	6.13	28.278
11	1040	146.27	−1.06	34.562	6.45	28.306	240	−1.14	34.555	6.49	28.307
12	1700	146.27	−0.48	34.632	5.76	28.306	125	−0.54	34.624	5.84	28.306
18	2215	146.27	−0.52	34.646	5.75	28.333	35	−0.51	34.647	5.74	28.333
19	2412	146.27	−0.61	34.641	5.65	28.342	32	−0.54	34.649	5.57	28.340
23	986	145.35	−1.56	34.519	6.70	28.333	136	−1.47	34.525	6.61	28.321
22	1347	145.38	−0.61	34.603	5.77	28.283	447	−0.65	34.598	5.82	28.278
21	2497	145.42	−0.85	34.606	5.95	28.346	87	−0.85	34.606	5.95	28.346
20	2886	145.43	−0.42	34.663	5.49	28.335	36	−0.42	34.662	5.49	28.335
28	1059	144.57	−1.09	34.556	6.25	28.298	329	−1.07	34.556	6.25	28.285
41	1352	144.53	−0.36	34.635	5.55	28.282	132	−0.38	34.632	5.58	28.282
42	2039	144.52	−0.70	34.605	5.87	28.317	119	−0.69	34.606	5.86	28.316
43	2530	144.44	−0.69	34.619	5.82	28.334	280	−0.69	34.618	5.82	28.333
34	809	143.50	−0.87	34.558	6.10	28.231	289	−0.94	34.551	6.18	28.226
30	1051	144.02	−1.56	34.515	6.71	28.323	121	−1.54	34.516	6.71	28.319
47	1124	143.75	−0.27	34.632	5.49	28.252	204	−0.29	34.628	5.52	28.248
46	1406	143.76	−0.45	34.626	5.63	28.288	156	−0.51	34.616	5.70	28.283
45	1876	143.73	−0.35	34.661	5.46	28.318	76	−0.33	34.661	5.46	28.316
44	2140	143.75	−0.99	34.589	6.14	28.346	180	−0.97	34.587	6.14	28.341
73	902	142.90	−1.22	34.624	6.37	28.396	67	−1.01	34.614	6.16	28.360
74	1212	142.88	−0.97	34.600	6.13	28.346	32	−0.97	34.599	6.09	28.344
75	1494	142.87	−0.73	34.597	5.77	28.305	34	−0.74	34.596	5.76	28.306
76	1773	142.81	−0.69	34.622	5.65	28.332	113	−0.67	34.622	5.64	28.328
77	2105	142.83	−0.93	34.593	5.89	28.343	235	−0.94	34.592	5.90	28.341
78	2459	142.89	−0.79	34.611	5.73	28.342	309	−0.60	34.636	5.53	28.335

formation by blocking the westward advection of sea ice, generating 'lee' polynyas for enhanced sea ice production/brine rejection. The MGT was also an important barrier between the water masses and circulations of the Adélie and Mertz Depressions, influencing the dual-system of dense shelf water export and overflows detailed in this paper. As of the 25th March it appears that B9b has re-grounded on the Ninnis Bank parallel to the coast and that C28, while still moving, is likely to become grounded near the Adélie Bank before the 2010 polynya season. In the long-term both icebergs are likely to break-up and leave the region with a new MGT re-emerging in the next 50–100 years. The impacts of these changes on the nature and variability of local sea-ice formation, dense shelf water export and AABW production from this region is the focus of current modelling work (pers comm. K. Kusahara). Given that this type of event is likely to regularly occur on pentadal to centennial timescales, it is important to consider these impacts on the temporal variability of AABW in the global ocean and climate system.

Appendix A: CTD Bottom Layer Properties

[77] In Tables A1 and A2 we present the bottom layer properties for CTD stations on the continental slope and rise from NBP00–08 and NBP04–08, respectively. Following *Muench et al.* [2009] we define the bottom layer thickness H_b and present water mass properties at the bottom (subscript "*b*") and averaged across the bottom layer H_b (subscript "*h*"). *Muench et al.* [2009] used the inflection point in $\theta - S$ space between CDW and cold, saline AABW. This method was less effective for the AGVL region, where there is ambient AABW and the local AABW is a cold and fresh end-member that does not offer a clear inflexion point (see Figure A1). Therefore we choose H_b (open circles in Figure A1) as the bottom mixed layer from vertical profiles, in a manner similar to *Girton and Sanford* [2003].

[78] **Acknowledgments.** This work was supported by the Japanese Society for the Promotion of Science Post Doctoral Fellowship program in conjunction with the Australian Academy of Science. Some or all of the data used within this paper were obtained from the Australian Antarctic Data Centre (IDN Node AMD/AU), a part of the Australian Antarctic Division (Commonwealth of Australia). These data are described in the metadata record "A bathymetric Digital Elevation Model (DEM) of the George V and Terre Adelie continental shelf and margin" (2009). The ALOS PALSAR data were provided by the Japan Aerospace Exploration Agency. Support for the NBP00–08 and NBP04–08 research voyages was provided by the U.S. National Science Foundation with the data processed and archived with the National Oceanographic Data Center. Support for the Mertz Polynya Experiment was provided by the Australian National Antarctic Research Expeditions, ASAC grant 2223. The authors would like to thank the officers and crew of the RVIB *Nathaniel B Palmer* and R/V *Aurora Australis* for their professional support in the collection of these observational data. In addition, the authors would like to thank Yasushi Fukamachi and Mark Rosenberg for helpful discussions.

References

Aoki, S., S. Rintoul, S. Ushio, and S. Watanabe (2005), Freshening of the Adélie Land Bottom Water near 140°E, *Geophys. Res. Lett.*, *32*, L23601, doi:10.1029/2005GL024246.

Assmann, K. M., and R. Timmermann (2005), Variability of dense water formation in the Ross Sea, *Ocean Dyn.*, *55*, 68–87.

Baines, P. G. (2008), Mixing in downslope flows in the ocean—Plumes versus gravity currents, *Atmos. Ocean*, *46*(4), 405–419.

Baines, P. G. (2009), A model for the structure of the Antarctic Slope Front, *Deep Sea Res., Part II*, 56, 859–873, doi:10.1016/j.dsr.2008.10.030.

Baines, P. G., and S. Condie (1998), Observations and modelling of Antarctic downslope flows: A review, in *Ocean, Ice, and Atmsophere: Interactions at the Antarctic Continental Margin*, *Antarctic Res. Ser.*, vol. 75, edited by S. S. Jacobs and R. F. Weiss, pp. 29–49, AGU, Washington, D. C.

Bindoff, N. L., G. D. Williams, I. Alison (2001), Sea-ice growth and water-mass modification in the Mertz Glacier polynya, East Antarctica, during winter, *Ann. Glaciol.*, *33*, 399–406.

Budillon, G., and G. Spezie (2000), Thermohaline structure and variability in the Terra Nova Bay polynya, Ross Sea, *Antarct. Sci.*, *12*, 493–508.

Buffoni, G., A. Cappelletti, and P. Picco (2002), An investigation of convection processes in Terra Nova Bay polynya, *Antarct. Sci.*, *4*, 79–89.

Carbulotto, A., L. De Santis, C. Zanolla, A. Camerlenghi, and J. Dix (2006), New insights into Quaternary glacial dynamic changes on the George V Land continental margin (East Antarctica), *Quat. Sci. Rev.*, *25*, 3029–3049.

De Santis, L., G. Brancolini, D. Accettella, A. Cova, A. Caburlotto, F. Donda, C. Pelos, F. Zgur, and M. Presti (2007), New insights into submarine geomorphology and depositional processes along the George V Land continental slope and upper rise (East Antarctica), in *Antarctica: A Keystone in a Changing World–Proceedings of the 10th International Symposium on Antarctic Earth Sciences*, edited by A. Cooper et al., *U.S. Geol. Surv., Open-File Rep. 2007-1047*, Extended Abstract 061, 5 pp.

Domack, E. W., and J. B. Anderson (1983), Marine geology of the George Vth Land continental margin: Combined results of the Deep Freeze 79 and the 1911–1914 Australian expedition, in *Antarctic Earth Science*, edited by R. L. Oliver et al., pp. 402–406, Cambridge Univ. Press, Cambridge, U. K.

Erofeeva, S. Y., G. Egbert, and L. Padman (1997), Assimilation of ship-mounted ADCP data for barotropic tides: Application to the Ross Sea, *J. Atmos. Oceanic Technol.*, *22*(6), 721–734.

Foldvik, A., T. Gammelsrd, S. Østerhus, E. Fahrbach, G. Rohardt, M. Schröder, K. W. Nicolls, L. Padman, R. A. Woodgate (2004), Ice shelf water overflow and bottom water formation in the southern Weddell Sea, *J. Geophys. Res.*, *109*, C02015, doi:10.1029/2003JC002008.

Fukamachi, Y., et al. (2000), Seasonal variability of bottom water properties off Adélie Land, Antarctica, *J. Geophys. Res.*, *105*, 6531–6540.

Gill, A. E. (1973), Circulation and bottom water formation in the Weddell Sea, *Deep Sea Res.*, *20*, 111–140.

Girton, J. B., and T. Sanford (2003), Descent and modification of the overflow plume in the Denmark Strait, *J. Phys. Oceanogr.*, *33*, 1351–1364.

Gordon, A. L., and P. Tchernia (1972), Waters of the continental margin off Adélie coast, Antarctica, in *Antarctic Oceanolgy II: The Australian-New Zealand Sector*, *Antarct. Res. Ser.*, vol. 19, edited by D. E. Hayes, pp. 59–69, AGU, Washington, D. C.

Gordon, A. L., E. Zambianchi, A. Orsi, M. Visbeck, C. F. Giulivi, T. Whitworth III, and G. Spezie (2004), Energetic plumes over the western Ross Sea continental slope, *Geophys. Res. Lett.*, *31*, L21302, doi:10.1029/2004GL020785.

Gordon, A. L., A. Orsi, R. Muench, B. A. Huber, E. Zambianchi, and M. Visbeck (2009), Western Ross Sea continental slope gravity currents, *Deep Sea Res., Part II*, *56*, 796–817, doi:10.1016/j.dsr.2008.10.037.

Ivanov, V., G. Shapiro, J. Huthnance, D. Aleynik, P. Golovin (2004), Cascades of dense shelf water around the world ocean, *Prog. Oceanogr.*, *60*, 47–98.

Jackett, D. R., and T. J. McDougall (1997), A neutral density variable for the world's oceans, *J. Phys. Oceanogr.*, *27*, 237–263.

Jacobs, S. S. (1991), On the nature and significance of the Antarctic Slope Front, *Mar. Chem. 35*(1–4), 9–24.

Jacobs, S. S. (2004), Bottom water production and its links with the thermohaline circulation, *Antarct. Sci.*, *16*, 427–437, doi:10.1017/S095410200400224X.

Jacobs, S. S. (2006), Observations of change in the Southern Ocean, *Philos. Trans. R. Soc.*, *364*, 1657–1681.

Jacobs, S. S., and C. F Giulivi (2010), Large multi-decadal salinity trends near the Pacific Antarctic continental margin, *Journal of Climate*, doi:10.1175/2010JCLI3284.1, in press.

Jacobs, S. S., C. F. Guilivi, and P. Mele (2002), Freshening of the Ross Sea during the late 20th century, *Science*, *297*, 386–389.

Kämpf, J. (2005), Cascading-driven upwelling in submarine canyons at high latitudes, *J. Geophys. Res.*, *110*, C02007, doi:10.1029/2004JC002554.

Kurtz, D. D., and D. H. Bromwich (1985), A recurring atmospherically forced polynya in Terra Nova Bay, in *Oceanology of the Antarctic Continental Shelf, Antarct. Res. Ser.*, vol. 43, edited by S. S. Jacobs, pp. 227–252, AGU, Washington, D. C.

Legrésy, B., A. Potzsch, I. Tabacco, F. Rémy, and R. Dietrich (2004), Influence of tides and tidal currents on the Mertz Glacier, East Antarctica, *J. Glaciol.*, *50*, 427–435.

Marsland, S. J., N. L. Bindoff, G. D. Williams, and W. F. Budd (2004), Modeling water mass formation in the Mertz Glacier polynya and Adélie

Depression, East Antarctica, *J. Geophys. Res.*, *109*, C11003, doi:10.1029/2004JC002441.
Marsland, S. J., J. Church, N. L. Bindoff, and G. D. Williams (2007), Antarctic coastal polynya response to climate change, *J. Geophys. Res.*, *112*, C07009, doi:10.1029/2005JC003291.
Massom, R. (2003), Recent iceberg calving events in the Ninnis Glacier Region, East Antarctica, *Antarct. Sci.*, *15*, 303–313.
Massom, R., K. Michael, P. T. Harris, and M. J. Potter (1998), The distribution and formative processes of latent heat polynyas in East Antarctica, *Ann. Glaciol.*, *27*, 420–426.
Massom, R., K. Hill, V. I. Lytle, A. P. Worby, M. J. Paget, I. Alison (2001), Effects of regional fast-ice and iceberg distributions on the behavior of the Mertz Glacier Polynya, East Antarctica, *Ann. Glaciol.*, *33*, 391–398.
Muench, R. D., L. Padman, A. L. Gordon, and A. Orsi (2009), A dense shelf outflow from the Ross Sea, Antarctica: Mixing and the contribution of tides, *J. Mar. Syst.*, *77*, 369–387, doi:10.1016/j.jmarsys.2008.11.003.
Orsi, A. H., and C. L. Wierderwohl (2009), A recount of Ross Sea waters, *Deep Sea Res., Part II*, *56*, 778–795.
Orsi, A. H., W. M. Smethie, and J. B. Bullister (2002), On the total input of Antarctic waters to the deep ocean: A preliminary estimate from chlorofluorocarbon measurements, *J. Geophys. Res.*, *107*(C8), 3122, doi:10.1029/2001JC000976.
Padman, L., S. L. Howard, A. H. Orsi, and R. Muench (2009), Tides of the northwestern Ross Sea and their impact on dense outflows of Antarctic Bottom Water, *Deep Sea Res., Part II*, *56*, 818–834.
Pawlowicz, R., B. Beardsley, and S. Lentz (2002), Classical tidal harmonic analysis including error estimates in MATLAB using t_tide, *Comput. Geosci.*, *28*, 929–937.
Price, J. F., and M. O. Baringer (1994), Outflows and deep water production by marginal seas, *J. Phys. Oceanogr.*, *33*, 1062–1079.
Rintoul, S. R. (1998), On the origin and influence of Adélie Land Bottom Water, in *Ocean, Ice, and Atmosphere: Interactions at the Antarctic Continental Margin*, *Antarct. Res. Ser.*, vol. 75, edited by S. Jacobs and R. Weiss, pp., 151–171, AGU, Washington, D. C.
Rintoul, S. R. (2007), Rapid freshening of Antarctic Bottom Water formed in the Indian and Pacific oceans, *Geophys. Res. Lett.*, *34*, L06606, doi:10.1029/2006GL028550.
Rodman, M., and A. L. Gordon (1982), Southern Ocean bottom water of the Australian-New Zealand sector, *J. Geophys. Res.*, *87*, 5771–5778.
Rosenberg, M. A., N. L. Bindoff, C. Curran, I. Helmond, K. Miller, D. Lachlan, J. Church, J. Richman, and H. Leffanue (2002), Amery Ice Shelf Experiment (AMISOR), Marine Science Cruises AU0106 and AU0207 - Oceanographic Field Measurements and Analysis, *Antarct. CRC Res. Rep. 30*, 119 pp., Coop. Res. Cent. for Antarct. and the Southern Ocean, Univ. of Tasmania, Hobart, Australia.
Swaters, G. E. (2006), On the frictional destabilization of abyssal overflows dynamically coupled to internal gravity waves, *Geophys. Astrophys. Fluid Dyn.*, *100*, 1–24.
Swaters, G. E. (2009a), Mixed bottom-friction-Kelvin-Helmholtz destabilization of source-driven abyssal overflows in the ocean, *J. Fluid Mech.*, *626*, 33–67.
Swaters, G. E. (2009b), Ekman destabilization of inertially-stable baroclinic abyssal flow on a sloping bottom, *Phys. Fluids*, *21*, 1–10.
Tamura, T., K. I. Ohshima, T. Markus, D. Cavalieri, S. Nihashi, and N. Hirasawa (2007), Estimation of thin ice thickness and detection of fast ice from SSM/I data in the Antarctic Ocean, *J. Atmos. Oceanic Technol.*, *24*, 1757–1772.
Tamura, T., K. I. Ohshima, and S. Nihashi (2008), Mapping of sea ice production for Antarctic coastal polynyas, *Geophys. Res. Lett.*, *35*, L07606, doi:10.1029/2007GL032903.
Whitworth, T., III (2002), Two modes of bottom water in the Australian-Antarctic Basin, *Geophys. Res. Lett.*, *29*(5), 1073, doi:10.1029/2001GL014282.
Whitworth, T., III, and A. H. Orsi (2006), Antarctic Bottom Water production and export by tides in the Ross Sea, *Geophys. Res. Lett.*, *33*, L12609, doi:10.1029/2006GL026357.
Whitworth, T., III, A. Orsi, S.-J. Kim, J. W. D. Nowlin, and R. Locarnini (1998), Water masses and mixing near the Antarctic Slope Front, in *Ocean, Ice, and Atmsophere: Interactions at the Antarctic Continental Margin*, *Antarct. Res. Ser.*, vol. 75, edited by S. Jacobs and R. Weiss, pp. 1–27, AGU, Washington, D. C.
Williams, G. D. (2004), Adélie Land Bottom Water production, Ph.D. thesis, Univ. of Tasmania, Hobart, Australia.
Williams, G. D., and N. L. Bindoff (2003), Wintertime oceanography of the Adélie Depression, *Deep Sea Res., Part II*, *50*, 1373–1392.
Williams, G. D., N. L. Bindoff, S. J. Marsland, S. R. Rintoul (2008), Formation and export of dense shelf water from the Adélie Depression, East Antarctica, *J. Geophys. Res.*, *113*, C04039, doi:10.1029/2007JC004346.

S. Aoki, Institute of Low Temperature Science, Hokkaido Univ., Kita-19, Nishi-8, Kita-ku, Sapporo 060-0819, Japan.
N. L. Bindoff and T. Tamura, Antarctic Climate and Ecosystem Cooperative Research Centre, Sandy Bay, Tas 7005, Australia.
S. S. Jacobs, Lamont-Doherty Earth Observatory, PO Box 1000, 61 Rt. 9W, Palisades, NY 10964, USA.
S. R. Rintoul, Center for Marine and Atmospheric Research, CSIRO, GPO Box 1538, Hobart, Tas 7001, Australia.
G. D. Williams, Laboratoire d'Ocanographie et du Climat: Exprimentations et approches numriques, UMR 7159, Universit Pierre et Marie Curie/MNHN, IRD, Institut Pierre Simon Laplace, CNRS, Bote 100 - 4, place Jussieu, F-75252 Paris, CEDEX 05, France.